

1-1-2007

Structural, metamorphic, and geochronological constraints on alternating compression and extension in the Early Paleozoic Gondwanan Pacific margin, northeastern Australia

Christopher L. Fergusson
University of Wollongong, cferguss@uow.edu.au

R A Henderson

I. W. Withnall

C M Fanning

D. Phillips

See next page for additional authors

Follow this and additional works at: <https://ro.uow.edu.au/scipapers>



Part of the [Life Sciences Commons](#), [Physical Sciences and Mathematics Commons](#), and the [Social and Behavioral Sciences Commons](#)

Recommended Citation

Fergusson, Christopher L.; Henderson, R A; Withnall, I. W.; Fanning, C M; Phillips, D.; and Lewthwaite, K. J.: Structural, metamorphic, and geochronological constraints on alternating compression and extension in the Early Paleozoic Gondwanan Pacific margin, northeastern Australia 2007, 1-20.
<https://ro.uow.edu.au/scipapers/1202>

Structural, metamorphic, and geochronological constraints on alternating compression and extension in the Early Paleozoic Gondwanan Pacific margin, northeastern Australia

Abstract

The Ross-Delamerian orogenic belt formed along the early Paleozoic active Pacific margin of the newly merged Gondwana supercontinent. In its northern-most segment in the Townsville region of northeastern Australia, we have identified a short contractional phase of the Delamerian orogeny in the Argentine Metamorphics postdating formation of a mafic breccia with a U-Pb zircon age of 500 ± 4 Ma. Contraction was followed by widespread inferred extensional deformation with formation of flat-lying foliation, domal features, and amphibolite grade and greenschist retrograde metamorphism all synchronous with latest Cambrian to Early Ordovician extensional backarc volcanism, sedimentation and intrusions. One of these intrusions gives a U-Pb zircon age of 480 ± 4 Ma. Foliation related to the extensional deformation is cross-cut by a late granodiorite dyke with a U-Pb zircon age of 461 ± 4 Ma. Late east-west contractional deformation affected the higher grade part of the assemblage. In contrast to the Ross-Delamerian orogenic belt in the Transantarctic Mountains and southeastern Australia, the orogenic belt in northeastern Australia was affected by a short episode of contraction at ~ 495 Ma followed by long-lived backarc extension from ~ 490 Ma to 460 Ma with subsequent contractional deformation.

Keywords

Structural, metamorphic, geochronological, constraints, alternating, compression, extension, Early, Paleozoic, Gondwanan, Pacific, margin, northeastern, Australia, GeoQUEST

Disciplines

Life Sciences | Physical Sciences and Mathematics | Social and Behavioral Sciences

Publication Details

Fergusson, C. L., Henderson, R., Withnall, I., Fanning, C., Phillips, D. & Lewthwaite, K. (2007). Structural, metamorphic, and geochronological constraints on alternating compression and extension in the Early Paleozoic Gondwanan Pacific margin, northeastern Australia. *Tectonics*, 26 (3), 1-20.

Authors

Christopher L. Fergusson, R A Henderson, I. W. Withnall, C M Fanning, D. Phillips, and K. J. Lewthwaite

1 **Structural, metamorphic and geochronological constraints**
2 **on alternating compression and extension in the Early**
3 **Paleozoic Gondwanan Pacific margin, northeastern**
4 **Australia**

5

6

7 C. L. Fergusson¹, R. A. Henderson², I. W. Withnall³, C. M. Fanning⁴, D. Phillips⁵, and K. J.
8 Lewthwaite²

9

10 ¹School of Earth and Environmental Sciences, University of Wollongong, NSW 2522,
11 Australia.

12 ²School of Earth and Environmental Sciences, James Cook University, Townsville, QLD
13 4811, Australia.

14 ³Geological Survey of Queensland, Natural Resource Sciences, Department of Natural
15 Resources, Mines and Water, 80 Meiers Road, Indooroopilly QLD 4068, Australia.

16 ⁴PRISE, Research School of Earth Sciences, The Australian National University, ACT 0200,
17 Australia.

18 ⁵School of Earth Sciences, University of Melbourne, Vic. 3010, Australia.

19

20

21 Running Title: FERGUSSON ET AL.: COMPRESSION-EXTENSION IN AST AUSTRALIA

22

23 Index Terms: 8109 Continental tectonics: extensional, 8110 Continental tectonics: general,
24 1199 Geochronology – miscellaneous, 9330 Australia

25

26 Key words: tectonics, extension, backarc, geochronology, Tasman Orogenic Zone

27

28 The Ross-Delamerian orogenic belt formed along the early Paleozoic active Pacific
29 margin of the newly merged Gondwana supercontinent. In its northern-most segment in the
30 Townsville region of northeastern Australia, we have identified a short contractional phase of
31 the Delamerian orogeny in the Argentine Metamorphics postdating formation of a mafic
32 breccia with a U-Pb zircon age of 500 ± 4 Ma. Contraction was followed by widespread
33 inferred extensional deformation with formation of flat-lying foliation, domal features, and
34 amphibolite grade and greenschist retrograde metamorphism all synchronous with latest
35 Cambrian to Early Ordovician extensional backarc volcanism, sedimentation and intrusions.
36 One of these intrusions gives a U-Pb zircon age of 480 ± 4 Ma. Foliation related to the
37 extensional deformation is cross-cut by a late granodiorite dyke with a U-Pb zircon age of 461
38 ± 4 Ma. Late east-west contractional deformation affected the higher grade part of the
39 assemblage. In contrast to the Ross-Delamerian orogenic belt in the Transantarctic Mountains
40 and southeastern Australia, the orogenic belt in northeastern Australia was affected by a short
41 episode of contraction at ~ 495 Ma followed by long-lived backarc extension from ~ 490 Ma to
42 460 Ma with subsequent contractional deformation.

43

44

45 **1. Introduction**

46

47 Subduction zone arc and backarc regions are characterized by the input of orogenic heat
48 and are therefore more susceptible to contractional and extensional deformation than cratons
49 and platforms [Thompson *et al.*, 2001; Hyndman *et al.*, 2005]. Extensional tectonics in
50 continental backarc settings is associated with the development of metamorphic core
51 complexes and associated low-angle normal faults as in the Aegean Sea [Lister *et al.*, 1984;
52 Ring and Layer, 2003] and the Basin and Range Province of southwestern North America
53 [Crittenden *et al.*, 1980]. In some regions extensional deformation has produced low-angle
54 intense foliation without formation of low-angle normal faults as in Hercynian low-pressure
55 amphibolite-grade metamorphics of the Pyrenees [Gibson, 1991] and greenschist to
56 amphibolite grade rocks in the Yukon-Tanana terrane of Alaska [Pavlis and Sisson, 1993].
57 Contractional deformation in continental backarc regions is most exemplified by late Miocene
58 to Recent foreland fold-thrust belts in the Andean backarc [Babeyko and Sobolev, 2005].
59 Alternating episodes of contraction and extension are widely recognized processes associated
60 with convergent margins [e.g., Hall, 2002].

61 The Tasman Orogenic Zone of eastern Australia (Figure 1) has formed along the active
62 Pacific-facing margin of East Gondwana [Cawood, 2005 and references therein] and has been
63 categorized as an extensional accretionary orogen with multiple episodes of arc and backarc
64 rifting interspersed with shorter episodes of contraction [Collins, 2002]. Cambrian to Early
65 Ordovician development of the Tasman Orogenic Zone is related to the Ross-Delamerian
66 orogenic belt that extends from northeastern Australia through the Adelaide Fold Belt of
67 southeastern Australia and into Victoria Land and the Central Transantarctic Mountains of
68 East Antarctica. Recognition of Delamerian orogenic events in northeastern Australia is only
69 recent with K-Ar ages of about 500 Ma for metamorphism and deformation in the Anakie
70 Metamorphic Group of central Queensland [Withnall *et al.*, 1996] and U-Pb zircon ages of

71 about 507–455 Ma for granitic intrusions in the Charters Towers Province of north
72 Queensland [Hutton *et al.*, 1997].

73 We have re-evaluated the structure and metamorphism of, and obtained
74 geochronological constraints for, the Argentine Metamorphics of the Charters Towers
75 Province in northeastern Australia (Figure 1). The new data enable us to establish the tectonic
76 history for this part of the Ross-Delamerian orogenic belt. A significant episode of post-
77 contraction extensional deformation has been recognized in the region, and building on prior
78 work [Fergusson *et al.*, 2005] we place this event in the context of extensional events
79 associated with Ross-Delamerian orogenesis as a whole. Cambrian to Early Ordovician
80 tectonism for the Ross-Delamerian orogenic belt has been characterized by broad-scale
81 contemporaneity of alternating extensional and contractional episodes [Foster *et al.*, 2005;
82 Squire and Wilson, 2005]. The tectonic synthesis presented herein incorporating data from the
83 northern Tasman Orogenic Zone confirms this alternation of tectonic mode but indicates more
84 complexity in space-time patterning than previously recognized for the East Gondwana
85 margin during 50 Ma of plate convergence and subduction in the Late Cambrian through the
86 Middle Ordovician.

87

88

89 **2. Regional Setting**

90

91 The northern Tasman Orogenic Zone consists of a Neoproterozoic to Early Paleozoic
92 assemblage developed in a northern equivalent of the Adelaide Fold Belt known as the
93 Thomson Fold Belt (Figure 1). Much of the Thomson Fold Belt is in the subsurface but
94 exposure occurs in the Anakie Inlier and the Charters Towers Province of central and north

95 Queensland respectively [*Murray and Kirkegaard, 1978*]. Early Paleozoic rocks also occur in
96 parts of the adjoining outboard Hodgkinson – Broken River Fold Belt but this belt is
97 dominated by Middle and Late Paleozoic rocks and it should be kept separate from the
98 Thomson Fold Belt [*cf. Glen, 2005*]. The Charters Towers Province of *Henderson* [1980] has
99 the most extensive and diverse rock systems of Ordovician age or older in the northern
100 Tasman Orogenic Zone. These older rocks include a belt of generally little deformed Late
101 Cambrian – Early Ordovician volcano-sedimentary rocks of the Mount Windsor Subprovince
102 [*Henderson, 1986*] and numerous granitoid phases of the Ravenswood Batholith and Fat Hen
103 Creek Complex that are largely Ordovician (507–455 Ma) and separated as the Macrossan
104 Igneous Province by *Hutton et al.* [1997] on the basis of age. Dispersed metamorphic tracts
105 form country rock to the Ordovician granitoids (Figure 2). They include the Cape River,
106 Running River, and Argentine Metamorphics as well as some smaller screens within the
107 Ravenswood Batholith.

108 Such metamorphics are the lowest structural unit in the Charters Towers Province and
109 consist of an assemblage of low to high-grade metasedimentary units with associated foliated
110 igneous rocks. Detailed geochronology is sparse [*e.g., Fergusson et al., 2005*]. An Early
111 Silurian orogenic event has been recognized for the southwestern Hodgkinson – Broken River
112 Fold Belt [*Arnold and Henderson, 1976*], affecting diverse rock systems that include Early
113 Ordovician siliceous turbidites, Late Ordovician volcanic and volcanoclastic rocks, and mafic-
114 ultramafic rocks of uncertain age [*Withnall and Lang, 1993*]. The Greenvale Province occurs
115 west of the Hodgkinson – Broken River Fold Belt (Figure 2) and contains tectonized Early
116 Paleozoic rock assemblages [*Nishiya et al., 2003*]. The Anakie Metamorphic Group,
117 extensively exposed as a basement inlier surrounded by interior basins of the northern New
118 England Fold Belt (Figure 1), is considered to represent an extension of the Delamerian

119 orogeny in northeastern Australia [*Withnall et al.*, 1996; *Fergusson et al.*, 2001]. Detrital
120 zircon age signatures indicate that these metamorphic units of the Thomson Fold Belt include
121 a latest Neoproterozoic passive margin succession and a younger, Cambrian stratigraphic unit
122 [*Fergusson et al.*, 2001, 2007].

123 The Argentine Metamorphics [*Withnall and McLennan*, 1991; *Hutton et al.*, 1997] are a
124 multiply deformed metasedimentary and metaigneous assemblage that forms many inliers
125 west of Townsville with the most significant being at Laroona (Figure 2) and in the Argentine
126 area (Figure 3). They are non-conformably overlain by, and faulted against, Devonian-
127 Carboniferous volcanic and sedimentary rocks of the Burdekin Basin. Deformation is
128 particularly evident in the sedimentary units of the lower less volcanic part of the Burdekin
129 Basin with syn-depositional extensional structures (half-graben and graben fill) and later
130 contractional structures although usually of low strain and associated with varying fold trends
131 [*Hutton et al.*, 1997]. Dips in these rocks are typically around 20–40° and it is likely that the
132 regional dips of the main foliation in the Argentine Metamorphics have been steepened during
133 contractional and/or extensional deformation of the overlying Burdekin Basin. Abundant
134 Carboniferous to Permian granitic intrusions and associated volcanic rocks are widespread in
135 the Charters Towers Province.

136

137

138 **3. Argentine Metamorphics**

139

140 Metasedimentary rocks dominate the assemblage with biotite schist, phyllite, minor
141 graphitic schist, quartzose metasandstone, quartzite, para-amphibolite and calcsilicate rock.
142 Metaigneous lithologies include foliated to massive amphibolite, mafic schist, serpentinite,

143 biotite/muscovite orthogneiss, migmatite and sills and dykes of leucogranite. We have
144 conducted detailed traverses across the unit mainly in the Argentine area (Figure 3) leading to
145 some revision of previously established units [*Withnall and McLennan*, 1991]. Major
146 subdivision is into higher grade and lower grade metamorphic packages. The higher grade
147 rocks occur in the northwestern to eastern part of Figure 3 and are dominated by paragneiss
148 and schist (Amg on Figure 3), including abundant quartzose metasandstone with granitic
149 veins, with adjoining orthogneiss (Amo). The lower grade package dominated by biotite
150 schist, quartzite (Ams) and mafic schist occurs in the southwestern part of Figure 3 and is also
151 mapped in other inliers of the Argentine Metamorphics [*Withnall and McLennan*, 1991] such
152 as at Laroon to the northwest (Figure 2). In the upper Cattle Creek area higher grade rocks
153 surround a core of phyllite that also contains some mafic schist (Figure 3). Ravenswood
154 Granodiorite has intruded metasedimentary gneiss and schist units to the southeast (Figure 3)
155 and is strongly foliated.

156 The primary sedimentary assemblage consisted predominantly of pelite interbedded
157 with quartz-intermediate sandstone, quartz-rich sandstone, and variably calcareous lithologies
158 that presumably are of marine origin. The small size of some amphibolite bodies suggests that
159 these rocks most likely represent a hypabyssal basic igneous assemblage whereas other
160 amphibolites may represent either a volcanic or a volcanoclastic protolith. Geochemistry
161 presented by *Withnall and McLennan* [1991] and summarized by *Hutton et al.* [1997] in
162 addition to further analyses on samples collected during this study [*Geological Survey of*
163 *Queensland*, 2005] suggest that two suites of mafic rocks are present in the Argentine
164 Metamorphics. The mafic schist associated with the low-grade package (Ams) shows
165 enrichment in high-field-strength elements similar to alkali basalts in intraplate settings,
166 whereas the amphibolite in interlayered schist and amphibolite (Amsa) show a relatively un-

167 enriched pattern and have tholeiitic affinities. *Withnall et al.* [1995] found a similar
168 divergence in geochemical affinities between mafic suites in the Anakie Metamorphic Group.

169

170

171 **3.1. Structure**

172 The Argentine Metamorphics are affected by up to four deformations whose
173 characteristics are given in Table 1 with orientation data shown in Figures 3–5. The highest-
174 grade metamorphic rocks along the abandoned Greenvale-Yabulu railway in the western part
175 of the Argentine area have the greatest structural complexity whereas the lower grade rocks
176 are simpler with the main foliation dipping away from the core of higher grade rocks (Figures
177 3 and 4). Lower grade rocks show two main deformations with S_1 foliation preserved in
178 microlithons associated with the regional S_2 (Figure 6a). Little is known about D_1 due to
179 strong overprinting by the D_2 deformation. D_2 formed the regional foliation (S_2) that mainly
180 dips moderately to gently southwards (Figures 3, 4 and 5a). Lithological layering is
181 commonly transposed subparallel to S_2 and tight folds abound (Figure 6b).

182 In the highest-grade rocks along the abandoned Greenvale-Yabulu railway in the
183 western part of the Argentine map area, microlithons in the main foliation are rare but occur
184 in some exposures. Banded orthogneiss in some zones of outcrop shows fine-scale (0.5–1 cm)
185 anastomosing layering indicative of high shear strain (mylonitic) fabrics and sporadic, narrow
186 (1–2 cm) zones of intense shear characterized by grain size reduction. The main foliation (S_2)
187 is more variable in orientation than at lower grades (Figure 3) due to overprinting D_3 and D_4
188 deformations. The D_3 deformation is mainly restricted to the area around the locality of
189 Argentine (Figure 3) and is manifest as tight to close, recumbent to gently inclined folds (Fig.
190 6c). The D_4 deformation is particularly prominent in the abandoned Greenvale-Yabulu

191 railway cuttings in the western part of the Argentine map area and has abundant F_4 folds
192 formed under east-west contraction.

193 The higher grade zone contains a domal feature defined by the orientation of S_2 in upper
194 Cattle Creek with an inner core of retrogressed lower grade rocks dominated by phyllite with
195 some mafic schist (Figures 3 and 4). In the core of the dome, foliation is nearly flat-lying
196 (Figure 5h). The phyllite is characteristically fine-grained in contrast to surrounding units and
197 contains widespread evidence for shearing such as folded lineations within the plane of the
198 foliation, S and C planes, and shear bands (Figure 6d). The fine grain size is attributed to
199 dynamic recrystallisation that accompanied shearing. Metamorphism has continued beyond
200 the major interval of shearing allowing recovery of grains and the development of strain-free
201 granoblastic aggregates in quartz-rich layers in the phyllite. All shear sense criteria are
202 consistent with top to the north and northeast.

203 Within deformed granitic plutons and coarser grained amphibolites intruding the
204 Argentine Metamorphics, a single main foliation is developed that has an orientation coplanar
205 with S_2 in the adjacent country rocks. The foliation has clearly formed by ductile deformation
206 and in granites is defined by aligned quartz, feldspar and clots of mainly chlorite that has
207 replaced the main mafic minerals.

208

209

210 **3.2. Metamorphism**

211 A general amphibolite grade peak of metamorphism for the Argentine Metamorphics is
212 indicated by garnet, and typically altered sillimanite and uncommon andalusite in pelitic rock
213 units and widespread hornblende and minor diopside in amphibolite, mafic schist and calc-
214 silicate rocks. In pelitic and psammopelitic rock types, micas and elongate quartz are aligned

215 along both S_1 and S_2 foliations indicating metamorphism accompanying these deformations.
216 In higher grade rocks S_1 is difficult to recognize in most outcrops and sillimanite, usually
217 replaced by muscovite, is aligned in the S_2 foliation but the relationship to S_1 is unknown.
218 Andalusite occurs in slightly lower grade rocks; it is also retrogressed and is aligned in the S_2
219 foliation. Retrogression is widespread with development of muscovite and chlorite.
220 Idioblastic garnets up to 2 mm across are locally developed in higher grade psammopelitic
221 gneisses rocks but lack inclusion trails. In most amphibolites a single foliation is defined by
222 aligned hornblende with elongate plagioclase and quartz (Figure 7). More rarely in some
223 amphibolites two foliations (S_1 , S_2) defined by elongate hornblende occur. Amphiboles
224 mainly have ferro-hornblende and ferro-tschermakite compositions. Some lithologies in thin
225 section show relict igneous clinopyroxene cores with amphibole rims, or clinopyroxene
226 partially replaced by amphibole.

227 Retrogression is also common in amphibolite and in some rocks actinolite and
228 tremolite have completely replaced all hornblende and clinopyroxene. Retrogression has been
229 partly synchronous with the second deformation in the lower grade rocks and the occurrence
230 of randomly oriented flakes of muscovite across foliation in some pelitic schist is consistent
231 with greenschist facies metamorphism continuing after the main phases of ductile
232 deformation. The development of andalusite and the lack of kyanite are consistent with low-
233 pressure metamorphism. Variation in the metamorphic grade is indicated by the widespread
234 development of migmatitic segregations and some pegmatitic veins in higher grade rocks and
235 their absence from lower grade rocks.

236 Temperatures of crystallization were determined from selected ilmenite-bearing
237 amphibolites and calc-silicate rocks using the edenite-richterite geothermometer of *Holland*
238 *and Blundy* [1994] and a method based on the TiO_2 content of amphibole devised by *Foster*

239 [in press]. Hornblende and plagioclase were analyzed using the JEOL JXA-8200 electron
240 probe microanalyser at James Cook University (mineral compositions and a full list of
241 calculated temperatures are available in the auxiliary materials). Temperature estimates
242 (Table 2) based on the TiO_2 thermometer of *Foster* [in press], generally indicate metamorphic
243 temperatures in the range of 540–590°C, consistent with lower to middle amphibolite facies
244 temperature estimates derived from thermodynamic considerations of the mineral
245 assemblages represented in the Argentine Metamorphics [see *Spear*, 1995]. However,
246 temperature estimates in the range of 730–770°C obtained from four samples are considered
247 to reflect relict igneous mineral compositional signatures which were not reset during
248 metamorphism. These samples are all medium-grained amphibolite with intergranular igneous
249 textures and phenocrysts ranging to 2 mm or more in diameter, and almost certainly are
250 metaplutonic rocks. In addition, three samples returning temperature estimates of 625–645°C
251 represent incomplete metamorphic resetting of igneous signatures.

252 With respect to the *Holland and Blundy* [1994] edenite-richterite geothermometer, only
253 three samples (A9, AM43 and AM91) returned estimates (527–583°C) that are plausible as
254 metamorphic temperatures with estimates for the other 11 samples anomalously high
255 (generally >655°C) with respect to the observed mineral assemblages, suggesting that the
256 method is not usefully applicable to the mineral chemistries of the rocks examined. This may
257 be due to the high iron content of the hornblendes analysed (generally 16–22% FeO), and
258 reflect difficulty in accurately assigning Fe_2O_3 contents calculated on the basis of
259 stoichiometry applied to microprobe analyses, with implications for other site fraction
260 allocations [see *Holland and Blundy*, 1994]. Alternatively, these amphibolites may have
261 formed from metamorphism of basic igneous rocks that intruded late in the metamorphic
262 episode and therefore were only partially equilibrated during metamorphism.

263

264

265 **4. Geochronology**

266 **4.1. Zircon U-Pb Age Data**

267 **4.1.1. Methods**

268 Samples were selected for U–Pb zircon dating by the Sensitive High Resolution Ion
269 Micro-Probe (SHRIMP at the Research School of Earth Sciences, Australian National
270 University). Zircons were separated from samples and cathodoluminescence images (CL)
271 were taken to enable selection of zircons for analysis on SHRIMP (Figure 8). Analytical
272 techniques followed methods given by *Williams* [1998] and references therein. Analyses
273 consisted of six scans through the mass range and results have been calibrated relative to
274 1099 Ma Duluth Gabbro reference zircons [*Paces and Miller*, 1993]. Data have been reduced
275 using the SQUID Excel Macro of *Ludwig* [2000] and plotted using ISOPLOT/EX [*Ludwig*,
276 1999]. All the areas analysed are <800 Ma and so common Pb correction has been made using
277 the measured $^{207}\text{Pb}/^{206}\text{Pb}$ and $^{238}\text{U}/^{206}\text{Pb}$ ratios as discussed in *Williams* [1998]. Therefore,
278 only radiogenic $^{206}\text{Pb}/^{238}\text{U}$ ratios and ages are reported in Tables 3–5. Some of the areas
279 analysed are considered discordant, having lost radiogenic Pb. Interpreted discordant analyses
280 have been excluded from weighted mean $^{206}\text{Pb}/^{238}\text{U}$ age calculations (Figure 9).

281 **4.1.2. Results**

282 Sample IWAM162D is a metaigneous clast within an amphibolite that comprises many
283 fragments and was probably a primary mafic volcanic breccia. It is from Towns Creek in the
284 Laroon area (Figure 2, 0393360 7861810 Ewan 8059 1:100 000 topographic map, map
285 datum AGD66) and was selected to provide a maximum age of deposition. The sample is very
286 fine-grained with quartz, plagioclase and minor biotite. The zircons from this clast are coarse

287 sub to anhedral grains for which CL scanning electron microscope images show broad
288 oscillatory zoning (Figure 8) as typical of those separated from less silicic igneous rocks such
289 as diorite [Hoskin, 2000]. The zircon has been affected by post magmatic effects and there
290 are thin ($\leq 5 \mu\text{m}$ in width) crack-seal veinlets filled with secondary zircon, too narrow to be
291 analyzed at this time. Twenty one areas on zoned magmatic zircon have been analyzed and
292 they all cluster within uncertainty of the Tera-Wasserburg Concordia curve, with the age
293 distribution forming a simple bell-shaped curve (Figure 9a, Table 3). All 21 analyses are
294 within analytical uncertainty giving a weighted mean $^{206}\text{Pb}/^{238}\text{U}$ age of $500 \pm 4 \text{ Ma}$ (2σ ;
295 $\text{MSWD} = 1.15$). This provides an estimate for the maximum time of formation of the breccia.

296 Sample HR1 is from a substantial body of coarse-grained, foliated granodiorite
297 cropping out in the southeastern extremity of the Argentine area (see Figure 3, 0431950
298 7843600 Dotswood 8158 1:100 000 topographic map) and was selected to provide a
299 maximum age of regional S_2 . Foliation is defined by elongate plagioclase and quartz with
300 seams of chloritized mafic minerals and is coplanar with the dominant (S_2) fabric in the
301 Argentine Metamorphics to the north. The zircons from this sample are euhedral grains with
302 simple oscillatory zonation under CL imaging (Figure 8b). Twenty zircon grains have been
303 analyzed (Figure 9b, Table 4); two are discordant and two others are significantly enriched in
304 common Pb. On the probability density plot it can be seen that there is a single dominant age
305 peak and the weighted mean for these 13 analyses is $480 \pm 4 \text{ Ma}$ (2σ ; $\text{MSWD} = 0.49$). This is
306 interpreted as the age of intrusion. Pervasive fabric development within the pluton suggests
307 that the D_2 deformation was active whilst elevated temperatures and thermal weakening
308 pertained during its cooling history at a time little separated from that of emplacement.

309 Sample AM77 is from a medium-grained granodiorite dyke exposed in a cutting on the
310 derelict railway line south of Cattle Creek (Figure 3, 0422500 7850410 Rollingstone 8159

311 1:100 000 topographic map) with weak S₄ but lacking the dominant foliation of the host
312 paragneiss. It contains altered plagioclase, quartz, minor biotite, rare garnet, scattered large
313 flakes of muscovite, and smaller flakes of muscovite replacing biotite and was selected to
314 provide a minimum age for S₂. The zircons from this sample are heterogeneous and have
315 complex internal structures. The CL images show a wide range of inherited components
316 forming the central areas to these grains, ranging from zoned magmatic to metamorphic
317 discrete areas (Figure 8c). Many grains have a dark CL, euhedral tip that is interpreted as
318 having formed at the time of intrusion of this granodiorite dyke. For the current study 25 areas
319 have been analyzed on 23 zircon grains, with the late stage dark CL tips being the target of
320 these analyses even though some of the areas are not ideal due to alteration. A number of the
321 areas analyzed are significantly enriched in common Pb (analysis 16.1 Table 5) or are
322 interpreted to have lost radiogenic Pb (analyses 3.1, 5.1, 21.1 and 23.1). On the relative
323 probability plot there is a dominant age peak that is skewed towards the younger side
324 reflecting the interpreted radiogenic Pb loss. A weighted mean for 13 analyses in this
325 dominant age peak gives an age of 461 ± 4 Ma (2σ ; Figure 9c, Table 5) and is considered to
326 date the time of magmatic zircon overgrowth. Thus intense deformation was substantially
327 completed by about 460 Ma.

328

329 **4.2. ⁴⁰Ar/³⁹Ar Age Data**

330 **4.2.1. Methods**

331 Sample AM89, an amphibolite (Figure 7) from the mafic schist/amphibolite unit in the
332 northern part of the Argentine area (~2 km north of map boundary near point A in Figure 3,
333 0420740 7856933 Rollingstone 8159 1:100 000 topographic map) was analyzed by the
334 ⁴⁰Ar/³⁹Ar method to provide a constraint on metamorphism of the Argentine Metamorphics.

335 Amphibole in this sample has a ferro-hornblende composition for which microprobe analyses
336 applied to geothermometry (Table 2) suggests retention of igneous compositional
337 characteristics. It was separated using conventional magnetic and heavy liquid separation
338 methods. Hand picking of the amphibole enabled a purity of greater than 99% to be achieved.
339 $^{40}\text{Ar}/^{39}\text{Ar}$ analyses were carried out at the School of Earth Sciences, The University of
340 Melbourne following procedures described previously by *Reid et al.* [2005]. The sample was
341 irradiated along with flux monitor Hb3gr hornblende (age = 1072 Ma; [*Turner et al.*, 1971;
342 *Roddick*, 1983]) in the McMaster University reactor, Canada. K_2SO_4 and CaF_2 salts were
343 included in the irradiation package to determine interference correction factors. After
344 irradiation, a weighed aliquot of the sample was loaded into a tin foil packet and step-heated
345 in a tantalum resistance furnace. $^{40}\text{Ar}/^{39}\text{Ar}$ step-heating analyses were conducted on a
346 VG3600 mass spectrometer, utilising a Daly detector. Mass discrimination values were
347 monitored by analyses of purified air aliquots. Correction factors for interfering isotopes are:
348 $(^{36}\text{Ar}/^{37}\text{Ar})_{\text{Ca}} = 2.79 (\pm 0.05) \times 10^{-4}$; $(^{39}\text{Ar}/^{37}\text{Ar})_{\text{Ca}} = 6.82 (\pm 0.05) \times 10^{-4}$; $(^{40}\text{Ar}/^{39}\text{Ar})_{\text{K}} = 0.0286$
349 ± 0.0006 . Decay constants are from *Steiger and Jäger* [1977].

350 **4.2.2. Results**

351 Amphibole from sample AM89 yielded a pseudo-plateau age of 438.7 ± 2.6 Ma (2σ ;
352 including J-error; MSWD = 0.79) that includes 46% of the ^{39}Ar (Figure 10, Table 6). This age
353 is similar to the mean value of 442.3 ± 5.0 Ma (2σ), obtained for all intermediate to high
354 temperature steps (1040 – 1450°C). Given that the amphibole composition is considered to
355 reflect igneous crystallization (Table 2) followed by strain during D_2 deformation (Figure 7),
356 which is constrained at between 460 and 480 Ma by the U-Pb data, the ~440 Ma result is
357 interpreted to indicate metamorphic cooling of the sample through the amphibole closure
358 temperature of ~500°C [e.g., *McDougall & Harrison*, 1999].

359

360

361 **5. Discussion and Conclusions**

362

363 **5.1. Tectonic Development of the Argentine Metamorphics**

364

365 Depositional attributes of the Argentine Metamorphics are poorly defined due to the
366 intensity of deformation and metamorphism. Deposition of the upper lower grade part of the
367 unit is probably Late Cambrian with a maximum limit to sedimentation and volcanism given
368 by the 500 ± 4 Ma clast from the Laroona area. On the basis of the youngest coherent group
369 of detrital zircons ages other late Middle to Late Cambrian quartzose successions are inferred
370 for the Thomson Fold Belt. These include the Halls Reward Metamorphics of the Greenvale
371 Province [*Nishiya et al.*, 2003], located 170 km west-northwest of the Argentine
372 Metamorphics, and the upper part of the Anakie Metamorphic Group in addition to a late
373 Neoproterozoic unit in the lower Anakie Metamorphic Group [*Fergusson et al.*, 2001], which
374 occur 300–400 km south of the Charters Towers Province.

375 Structural relationships between the higher grade and the lower grade rocks have been
376 disputed. *Hammond* [1986] inferred a detachment zone between these two packages but the
377 mapping of *Withnall and McLennan* [1991] and our work does not support this interpretation
378 and instead a gradational relationship is recognized. The style of early deformation in the
379 Argentine Metamorphics is obscured by the intensity of the D_2 deformation but given the
380 apparent steep orientation of the S_1 foliation, it is considered to reflect contractional
381 deformation. Timing of this event is bracketed between the inferred depositional age of the
382 upper Argentine Metamorphics and the intrusion of the adjoining granodiorite pluton which

383 was synchronous with the D₂ deformation (Figure 11). Intense D₂ deformation was
384 accompanied by this intrusion at 480 ± 4 Ma and postdated by a granodiorite dyke with an
385 age of 461 ± 4 Ma. D₃ and D₄ deformations are only found in the higher grade part of the
386 Argentine Metamorphics. D₄ deformation consists of upright, northerly trending structures
387 reflecting east-west contraction presumably accompanied by uplift and erosion and could be
388 responsible for the $^{40}\text{Ar}/^{39}\text{Ar}$ cooling age of ~ 440 Ma on amphibole from amphibolite from
389 the structurally lower part of the assemblage. In contrast both D₂ and D₃ deformations
390 developed with recumbent to near recumbent attitudes and therefore largely reflect vertical
391 flattening (see below). Our interpretation is that amphibolite facies metamorphism
392 accompanied deformation with high temperatures persisting in the higher grade part of the
393 unit up to the D₄ deformation. A clear spatial relationship exists between the higher grade
394 core of the Argentine Metamorphics dominated by partially sheet-like orthogneiss and rocks
395 with abundant granitic segregations and veins implying that the locally higher grade
396 conditions reflect heat advection associated with synchronous intrusions as widely
397 documented in low-pressure metamorphic terrains [*Richards and Collins, 2002; Caggianelli*
398 *and Prosser, 2002*].

399

400

401 **5.2 Role of Extensional Deformation**

402

403 The role of extensional deformation in the uplift of high pressure and ultra-high
404 pressure metamorphic rocks and in the exhumation of metamorphic core complexes is well
405 documented in the literature [e.g., *Crittenden et al., 1980; Ring and Layer, 2003*]. The
406 Argentine Metamorphics lack evidence for an extended brittle hanging wall block and no

407 detachment fault has been recognized. Suggestions of a detachment fault between the lower
408 grade and higher grade packages of rocks are not consistent with the widespread development
409 of amphibolite facies metamorphism throughout the unit. An extensional origin for the D₂
410 deformation accounts for the original flat-lying orientation of the main S₂ foliation with
411 abundant recumbent folds and extension within the foliation plane consistent with vertical
412 flattening. Comparable flat-lying foliation is a feature of regional developed amphibolite and
413 greenschist facies rocks of the Yukon-Tanana Terrane of east-central Alaska [*Pavlis and*
414 *Sisson, 1993*] and attributed to extensional tectonics. Sub-horizontal foliation in higher grade
415 rocks has also been widely attributed to vertical flattening of the lower crust during
416 extensional tectonics [*Sandiford, 1989; Harris et al., 2002*].

417 A problematic feature of the Argentine area is the development of the Cattle Creek
418 dome and its association with the D₃ deformation which is particularly evident on the
419 southern flank of the dome. The domal feature is also shown by the orientation of bedding in
420 the Devonian sedimentary cover (Figure 3) and is therefore partly due to post-Devonian upper
421 crustal deformation. D₃ structures are recumbent as inferred for development of the D₂
422 deformation, indicating continued vertical flattening. For new recumbent folds to develop
423 during D₃ the main S₂ foliation must have been tilted prior to the imposition of strain so that
424 the S₂ foliation lay in the shortening rather than extending field during progressive
425 deformation. This could have occurred only if the Cattle Creek dome developed during
426 continued vertical flattening that generated the D₂ and D₃ deformations. Such doming may
427 have formed as result of largescale boudinage and/or doming due to intrusion of an
428 underlying granitic and/or mafic mass synchronous with D₂; the lack of relict granitic veins in
429 the phyllite unit does not support the latter alternative. The position of intensely deformed
430 retrograde phyllite in the core of the Cattle Creek dome is consistent with the development of

431 the dome at the margin of a largescale boudin.

432 An origin for the D₂ and D₃ deformations based on the flat-lying orientation for
433 foliations in metamorphic rocks although widely related to extensional tectonics is not
434 conclusive as flat-lying foliations have also been documented in contractional settings such as
435 in the lower limbs of nappes in the western Alps [Ramsay *et al.*, 1983]. A contractional
436 setting is difficult to rule out entirely on the basis of field relationships but the problem can be
437 tackled by examining the regional relationships and setting of the Argentine Metamorphics.

438

439

440 **5.3 Regional Relationships – Metamorphic Rocks**

441

442 The Cape River Metamorphics located some 150 km southwest of the Argentine
443 Metamorphics (Figure 2) comprise a substantial tract in the western part of the Charters
444 Towers Province. They are similar to the Argentine Metamorphics in terms of rock types,
445 metamorphic grade, structural succession and association with syntectonic granitoid
446 emplacement [Hutton *et al.*, 1997]. An early contractional deformation was overprinted by
447 sub-horizontal intense D₂ fabrics which Fergusson *et al.* [2005] ascribed to extensional
448 tectonics. This in turn was followed by contractional deformation that formed northwest-
449 trending upright folds [Hutton *et al.*, 1997]. D₄ of the Argentine Metamorphics, associated
450 with northerly trending structures reflecting east-west shortening, is a comparable structural
451 phase. The Cape River Metamorphics have fewer age constraints than the Argentine
452 Metamorphics. Detrital zircons from metasediments of the Cape River Metamorphics are
453 typically ~900 Ma or older [Blewett *et al.*, 1998; Fergusson *et al.*, 2007] and only constrain
454 the depositional age to no older than Neoproterozoic. The unit is intruded by plutons of the

455 Fat Hen Creek Complex, the oldest of which is affected by the D₂ deformation and have U–
456 Pb zircon ages of 493–455 Ma (Figure 11) [Hutton *et al.*, 1997]. ⁴⁰Ar/³⁹Ar cooling ages for
457 biotite and muscovite for the Cape River Metamorphics are in the range 425–410 Ma which
458 corresponds to erosional exhumation following Early Silurian contraction expressed as the
459 final contractional deformation also evident in the Hodgkinson – Broken River Fold Belt to
460 the north [Fergusson *et al.*, 2005].

461 The Anakie Metamorphic Group located south of the Charters Towers Province within
462 the Anakie Inlier (Figure 1), represents exposure that is probably indicative of widespread
463 concealed basement throughout much of central Queensland [Withnall *et al.*, 1995]. It also
464 has a similar lithological content and structural succession to the Argentine Metamorphics.
465 Fergusson *et al.* [2005] have reinterpreted the major subhorizontal S₂ foliation developed in
466 the Anakie Metamorphic Group as reflecting extensional tectonics. An upper limit to the
467 timing of deformation of the Anakie Group is provided by several K/Ar ages on metamorphic
468 cooling and S₂ foliation development of ~500 Ma [Withnall *et al.*, 1996]. The youngest
469 detrital zircons from the upper part of the succession are ~510 Ma [Fergusson *et al.*, 2001]
470 and therefore deformation is constrained to an interval of 510–500 Ma implying a much
471 shorter deformational history compared to that of the Charters Towers Province.

472 Our data from the Argentine Metamorphics more concisely define the tectonic history
473 of the Charters Towers Province with implications for the Early Paleozoic metamorphic
474 basement throughout northeastern Australia. In summary, basement formed from a primary
475 succession with deposition continuing up until the earliest Late Cambrian at 500 ± 4 Ma
476 followed by contractional deformation and low-pressure metamorphism at ~495 Ma (Late
477 Cambrian) using the timescale of Gradstein and Ogg [2004]. This was followed by a major
478 episode of extensional tectonics from ~490 to 460 Ma as demonstrated by U-Pb zircon ages

479 for plutonic rocks in the Argentine Metamorphics. East-west contractional deformation
480 possibly around 440 Ma in the high-grade part of the Argentine Metamorphics appears to
481 have been of only local significance with regional uplift and metamorphic cooling
482 demonstrated in the latest Ordovician to Early Silurian by $^{40}\text{Ar}/^{39}\text{Ar}$ cooling ages for the Cape
483 River Metamorphics and syntectonic conglomeratic wedges in the southwestern Hodgkinson
484 – Broken River Fold Belt [Arnold and Henderson, 1976; Withnall and Lang, 1993; Fergusson
485 *et al.*, 2005; data herein].

486

487

488 **5.4 Regional Relationships – Upper Crustal Rocks**

489

490 The southern part of the Charters Towers Province, the Mount Windsor Subprovince
491 [Henderson, 1980], is dominated by a latest Cambrian to Early Ordovician succession of
492 sedimentary and volcanic rocks comprising the Seventy Mile Range Group [Henderson,
493 1986]. This is a succession of deep marine origin that includes a thick unit of silicic lavas and
494 pyroclastic rocks overlain by a mixed unit of silicic to mafic volcanics and volcanoclastics in
495 turn overlain by a thick lithic sedimentary succession. The age of the upper part of the group
496 is well established from graptolitic horizons above the main silicic volcanic unit that are of
497 Early Ordovician (Lancefieldian to Chewtonian) age [Henderson, 1983]. Given that a thick
498 volcanic and sedimentary interval occurs below the fossiliferous rocks, the lower part of the
499 Seventy Mile Group must extend into the Late Cambrian. Deposition of the group therefore
500 ranges from at least ~495 Ma to ~470 Ma (Figure 11) using the timescale of the *Gradstein*
501 *and Ogg* [2004].

502 The Seventy Mile Range Group occurs well to the south of the Argentine

503 Metamorphics. However they do abut the Cape River Metamorphics (Figure 2) but contact
504 relationships are difficult to resolve because of the intensity of late contractional deformation
505 that affects the Cape River Metamorphics and in this area the Seventy Mile Range Group
506 which for most of its extent is only weakly deformed. Volcanic and hypabyssal rocks of the
507 main part of the Seventy Mile Range Group have a magmatic signature consistent with an
508 extensional backarc setting [*Henderson, 1986; Stolz, 1995*]. Volcanic rocks within the oldest,
509 unfossiliferous sedimentary part of the Seventy Mile Range Group, the Puddler Creek
510 Formation, have geochemical affinities of an alkaline intraplate association [*Stolz, 1995*], like
511 the mafic schist in the lower-grade part of the Argentine Metamorphics [*Hutton et al., 1997*].
512 Syndepositional normal faulting has also accompanied deposition of the Seventy Mile Range
513 Group [*Berry et al., 1992*].

514 Thus the Charters Towers Province in the latest Cambrian to Early Ordovician (~490
515 Ma to ~460 Ma) had regional flat-lying foliation development in an extensional setting in the
516 mid to lower upper crust accompanied by extensional backarc volcanism and sedimentation in
517 the supracrustal rocks of the Seventy Mile Range Group (Figure 12). The province is
518 characterized by voluminous plutonic phases that comprise the Lolworth and Ravenswood
519 Batholiths, with the Late Cambrian to Late Ordovician Macrossan Igneous Province [507 to
520 455 Ma, *Hutton et al., 1997*] represented by dominantly granodiorite but ranging to gabbro
521 and tonalite. The age of this suite overlaps with that of the metamorphic assemblages and the
522 Seventy Mile Range Group (Figure 11).

523 These relationships are consistent with extensional thinning of the lithosphere whereby
524 the supracrustal zone experienced rifting and broadscale basin formation [*McKenzie, 1978*]
525 whereas deeper crustal levels experienced enhanced thermal gradients, high-T/low-P
526 metamorphism and thermo-mechanical weakening within a pure shear regime (Figure 12)

527 [e.g., *Thompson et al.*, 2001]. Large plutons, like that intruding the southeastern margin of
528 the Argentine Metamorphics which has an exposed area of some 100 km² and is doubtless
529 more extensive beneath Devonian sedimentary cover, generated predominantly in the
530 extensional regime enabled thermal energy to be transported upwards in the crust and
531 encouraged the development of high-T/low-P metamorphic assemblages [e.g., *Caggianelli*
532 *and Prosser*, 2002].

533

534

535 **5.5 Gondwanan Context**

536

537 Along the Australian sector of the Pacific-facing margin of East Gondwana it has been
538 argued by *Direen and Crawford* [2003] that rifting and continental separation at ~600 Ma
539 resulted in the development of a passive volcanic margin. This newly developed passive
540 margin is considered the site of deposition for some of the successions preserved in
541 northeastern Australia (e.g., lower Anakie Metamorphic Group [*Fergusson et al.*, 2001]) and
542 associated mafic igneous activity [*Withnall et al.*, 1995]. In contrast at least five episodes of
543 rifting, associated sedimentation and minor volcanism occurred between 827 Ma and 520 Ma
544 in the Adelaide Fold Belt of southeastern South Australia with continental separation
545 hypothesized at 700 Ma [*Preiss*, 2000]. An older age of continental separation in the Adelaide
546 Fold Belt is consistent with an age of 668 ± 1 Ma for gabbroic rocks associated with the
547 Beardmore Group of the Central Transantarctic Mountains and ~670 Ma detrital zircons in
548 the Koettlitz Group of Southern Victoria Land [*Goodge et al.*, 2002, 2004a]. Given the
549 association of inferred rift-related mafic volcanism and sediments with detrital zircons of
550 600–570 Ma age in the Anakie Metamorphic Group [*Withnall et al.*, 1995; *Fergusson et al.*,

551 2001], a single continental fragmentation event to form East Gondwana is not viable [cf.
552 *Pisarevsky et al.*, 2003]. Alternatively, fragmentation of a supercontinent was followed by
553 separation of one or more continental ribbons from parts of the East Gondwana margin, such
554 as northeastern Australia.

555 In the Middle Cambrian to Early Ordovician interval, Australia was part of the recently
556 amalgamated Gondwana continent formed from merger of East and West Gondwana, which
557 coincided with the development of an active margin along the Pacific-facing side of
558 Gondwana [*Boger and Miller*, 2004]. Contractional deformation is evident in the Middle to
559 Late Cambrian along much of the Ross-Delamerian orogenic belt (Figure 11)[*Stump*, 1995;
560 *Preiss*, 2000]. The Delamerian orogeny is considered to have affected eastern Australia
561 between 520 Ma and 490 Ma, and includes events such as fold-thrust belt development in the
562 western Adelaide Fold Belt with low-pressure metamorphism and contractional deformation
563 in the eastern Adelaide Fold Belt [*Preiss*, 2000; *Crawford et al.*, 2003]. In Tasmania,
564 ophiolite emplacement and high-pressure metamorphism in the Delamerian Orogeny at
565 515–508 Ma was followed by post-collisional extension at 508–495 Ma including
566 magmatism [*Foster et al.*, 2005]. In the Ross Orogen of the Transantarctic Mountains,
567 relatively long-lived contractional deformation has been prominent (Figure 11).

568 In northeastern Australia, contractional deformation associated with this convergence is
569 constrained to ~495 Ma (Figure 11), in contrast to southeastern South Australia where
570 Delamerian contractional deformation began around 514 ± 5 Ma [*Foden et al.*, 1999] and
571 continued into the Late Cambrian with an upper constraint provided by late undeformed
572 plutons at 490–485 Ma (Figure 11)[*Haines and Flöttmann*, 1998]. Extensional tectonics
573 occurred to the east in the Lachlan Fold Belt where Middle to Late Cambrian (520–495 Ma)
574 volcanic inliers contain rocks of backarc association [*Foster et al.*, 2005] and exhumation of

575 the Moornambool Metamorphic Complex at its western margin also attributed to extensional
576 tectonics is dated at ~500 Ma [Miller *et al.*, 2005]. Short-lived contraction in northeastern
577 Australia was followed by extensional tectonics in a continental backarc setting that
578 continued from ~490 Ma to ~460 Ma (i.e. latest Cambrian to the Middle/Late Ordovician
579 boundary). This extensional event is not recognized in South Australia and East Antarctica
580 but coincides with tectonic events in the Lachlan Fold Belt. The first phase of volcanic
581 activity associated with the Macquarie arc in the eastern Lachlan Fold Belt occurred at
582 ~485–480 Ma followed by renewed activity at ~470 Ma (Figure 11)[Glen *et al.*, 1998; Butera
583 *et al.*, 2001; Packham *et al.*, 2003]. During this interval widespread Early to Middle
584 Ordovician deposition of the vast ‘Bengal Fan-type’ turbidite deposits was more-or-less
585 continuous in the Lachlan Fold Belt and inundated Middle to Late Cambrian island arc and
586 backarc crust that developed outboard of the Ross-Delamerian orogenic belt [Fergusson and
587 Fanning, 2002; Crawford *et al.*, 2003]. Early Ordovician extensional tectonics in the
588 Australian part of East Gondwana is also indicated by extensional deformation in amphibolite
589 facies rocks of the Harts Range in central Australia [Hand *et al.*, 1999].

590 The role of extensional events during the Early to Middle Cambrian in association with
591 Ross-Delamerian orogenesis has been emphasized by Squire and Wilson [2005]. They argued
592 that a major short-lived (2 Ma) extensional event at ~515 Ma interrupted Early Cambrian
593 contraction and affected the entire Pacific margin of East Gondwana. This event was related
594 to roll-back of the subducting plate with development of juvenile arc boninitic and tholeiitic
595 mafic volcanic basement, in the sense of Stern [2002], in the Lachlan Fold Belt, Northern
596 Victoria Land, Tasmania, New Zealand and the Ellsworth Mountains of West Antarctica
597 [Squire and Wilson, 2005, figure 5]. While the formation of these volcanic rocks is well
598 constrained at several sites (e.g., the southern Heathcote greenstone belt of central Victoria

599 and Wellington greenstone belt at Wellington River in eastern Victoria), in most places
600 volcanism is only poorly dated and is indicated as only pre-latest Cambrian by fossils in the
601 upper part of the overlying pelagic sedimentary succession [e.g., VandenBerg *et al.*, 2000].
602 Hornblende gabbro in the Dookie complex of the northern Mount Wellington greenstone belt,
603 in central Victoria, has a U-Pb zircon age of 502 ± 0.7 Ma [Spaggiari *et al.*, 2003] equivalent
604 in age to a less widespread extensional event identified by Squire and Wilson [2005] at
605 505–500 Ma and indicating that the juvenile island arc basement of the Lachlan Fold Belt was
606 not constrained to one extensional event at ~515 Ma. Ti-poor ophiolitic rocks of the Weraerai
607 terrane in the southern New England Fold Belt have U-Pb zircon ages of ~530 Ma [Aitchison
608 *et al.*, 1992; Aitchison and Ireland, 1995] and these ages imply that there was a protracted and
609 probably dispersed development of juvenile island arc sea floor in the Pacific Ocean outboard
610 of the Ross-Delamerian active continental margin. Contraction has been interrupted by
611 extension along parts of the Pacific margin of East Gondwana such as during deposition of
612 the ~525 to 515 Ma Kanmantoo Group in an extensional basin that transected the ancient
613 passive margin in southeastern South Australia [Preiss, 2000]. For much of the East
614 Gondwana active margin, it is clear that convergent deformation in the Ross-Delamerian
615 orogenic belt and extensional tectonics in the adjoining Pacific realm were synchronous,
616 analogous at a smaller scale to the present-day Taiwan island arc collision and extension in
617 the Okinawa trough [Hall, 2002]. This is shown in several reconstructions from 520 Ma to
618 460 Ma where extensional regimes co-exist with contractional deformation along the Pacific
619 margin of Gondwana (Figure 13).

620 The post-extension, early Silurian contraction recognized herein as a widespread event
621 in north Queensland broadly correlates with shortening in the Lachlan Fold Belt dated as
622 occurring between 460 and 420 Ma [Foster *et al.*, 1999].

623

624

625 **5.6. Conclusions**

626

627 Metamorphic rocks in the Townsville region of northeastern Australia represent a
628 continuation of the Ross-Delamerian orogenic belt that formed along the paleo-Pacific margin
629 of Gondwana in the Cambrian to Ordovician. These rocks are an assemblage of siliciclastic
630 metasedimentary and metaigneous rocks with widespread amphibolite and include mafic
631 breccia with a minimum depositional age indicated by a U-Pb zircon age of 500 ± 4 Ma. They
632 were affected by poly-phase deformation with an accompanying metamorphic episode
633 reaching amphibolite facies conditions with anatexis in higher grade rocks. The first
634 deformation was contractional and considered related to widespread convergent deformation
635 along the active Gondwana margin in the Late Cambrian. The second deformation produced
636 intense originally flat-lying foliation and is constrained to an age of ~ 490 Ma to ~ 460 Ma by
637 two U-Pb zircon ages (480 ± 4 Ma and 461 ± 4 Ma) for granites affected by and postdating
638 the main foliation respectively. This deformation was synchronous with deposition further
639 south of late Cambrian to Early Ordovician sedimentary and volcanic rocks with a backarc
640 extensional tectonic affinity and therefore we interpret the flat-lying foliation (D_2
641 deformation) as a result of extensional tectonics [e.g., *Pavlis and Sisson, 1993*]. This
642 extensional episode was concurrent with the development of widespread juvenile island arc
643 and oceanic backarc crust in southeastern Australia and continuing convergent deformation
644 along the Ross-Delamerian orogenic belt. Final contractional deformation affected the higher
645 grade part these metamorphic rocks during long-lived uplift, widespread retrogression and
646 inferred metamorphic cooling.

647

648 **Acknowledgments.** Research funds were provided by the Australian Research
649 Council (grant number A00103036), with additional support from James Cook University, the
650 University of Wollongong and the Geological Survey of Queensland. We are grateful to the
651 Australian Army for allowing access to the Argentine training area. David Carrie made many
652 excellent thin sections. Peter Johnson computer drafted the figures. We thank Damien Foster for
653 assistance with metamorphic aspects during revision of the manuscript. Comments and
654 suggestions on the initial manuscript by two anonymous reviewers resulted in a much improved
655 manuscript.

656

657

658 **References**

659

660 Aitchison, J. C., T. R. Ireland, M. C. Blake, and P. G. Flood (1992), 530 Ma zircon age for
661 ophiolite from the New England orogen: oldest rocks known from eastern Australia.

662 *Geology*, 20, 125–128.

663 Aitchison, J. C. and T. R. Ireland (1995), Age profile of ophiolitic rocks across the Late

664 Paleozoic New England Orogen, New South Wales: implications for tectonic models, *Aust.*

665 *J. Earth Sci.*, 42, 11–23.

666 Allibone, A. H. and R. J. Wysoczanski (2002), Initiation of magmatism during the

667 Cambrian–Ordovician Ross orogeny in southern Victoria Land, Antarctica, *Geol. Soc.*

668 *Amer. Bull.*, 114, 1007–1018.

669 Arnold, G. O., and R. A. Henderson (1976), Lower Palaeozoic history of the southwestern

670 Broken River Province, North Queensland, *J. Geol. Soc. Aust.*, 23, 73–93.

- 671 Babeyko, A. Y., and S. V. Sobolev (2005), Quantifying different modes of the late Cenozoic
672 shortening in the central Andes, *Geology*, 33, 621–624.
- 673 Berry, R. F., D. L. Huston, A. J. Stolz, A. P. Hill, S. D. Beams, U. Kuronen, and A. Taube
674 (1992), Stratigraphy, structure, and volcanic-hosted mineralization of the Mount Windsor
675 Subprovince, North Queensland, Australia, *Econ. Geol.*, 87, 739–763.
- 676 Blewett, R. S., L. P. Black, S-S. Sun, J. Knutson, L. J. Hutton, and J. H. C. Bain (1998), U-Pb
677 zircon and Sm-Nd geochronology of the Mesoproterozoic of North Queensland:
678 implications for a Rodinian connection with the Belt supergroup of North America,
679 *Precambrian Res.*, 89, 101–127.
- 680 Boger, S. D., and J. McL. Miller (2004), Terminal suturing of Gondwana and the onset of the
681 Ross-Delamerian Orogeny: the cause and effect of an Early Cambrian reconfiguration of
682 plate motions, *Earth Planet. Sci. Lett.*, 219, 35–48.
- 683 Butera, K. M., I. S. Williams, P. L. Blevin, and C. J. Simpson (2001), Zircon U-Pb dating of
684 Early Palaeozoic monzonitic intrusives from the Goonumbla area, New South Wales,
685 *Aust. J. Earth Sci.*, 48, 457–464.
- 686 Caggianelli, A., and G. Prosser (2002), Modelling the thermal perturbation of the continental
687 crust after intraplating of thick granitoid sheets: a comparison with the crustal sections in
688 Calabria (Italy), *Geol. Mag.*, 139, 699–706.
- 689 Cawood, P. A. (2005), Terra Australis Orogen: Rodinia breakup and development of the Pacific
690 and Iapetus margins of Gondwana during the Neoproterozoic and Paleozoic, *Earth-Sci.*
691 *Rev.*, 69, 249–279.
- 692 Collins, W. J. (2002), Nature of extensional orogens, *Tectonics*, 21(4),
693 doi:10.1029/2000TC001272.
- 694 Crawford, A. J., R. A. Cayley, D. H. Taylor, V. J. Morand, C. M. Gray, A. I. S. Kemp, K. E.

- 695 Wohlt, A. H. M., VandenBerg, D. H., Moore, S., Maher, N. G., Direen, J., Edwards, A. G.
696 Donaghy, J. A., Anderson, and L. P. Black (2003), Neoproterozoic and Cambrian
697 continental rifting, continent-arc collision and post-collisional magmatism, in *The*
698 *Geology of Victoria*, edited by W. Birch, pp. 73–93, Geol. Soc. Aust., Victorian Division.
- 699 Crittenden, M. D., P. J. Coney, and G. H. Davis (Eds.) (1980), *Cordilleran Metamorphic Core*
700 *Complexes*, Geol. Soc. Am. Mem., 153, 490 pp., Boulder, CO.
- 701 Dallmeyer, R. D., and T. O. Wright (1992), Diachronous cleavage development in the
702 Robertson Bay terrane, Northern Victoria Land, Antarctica: tectonic implications,
703 *Tectonics*, 11, 437–448.
- 704 Direen, N. G., and A. J. Crawford (2003), Fossil seaward-dipping reflector sequences
705 preserved in southeastern Australia: a 600 Ma volcanic passive margin in eastern
706 Gondwanaland, *J. Geol. Soc. London*, 160, 985–990.
- 707 Fergusson, C. L., and C. M. Fanning (2002), Late Ordovician stratigraphy, zircon provenance
708 and tectonics, Lachlan Fold Belt, southeastern Australia, *Aust. J. Earth Sci.*, 49, 423–436.
- 709 Fergusson, C. L., P. F. Carr, C. M. Fanning, and T. J. Green (2001), Proterozoic-Cambrian
710 detrital zircon and monazite ages from the Anakie Inlier, central Queensland: Grenville
711 and Pacific-Gondwana signatures, *Aust. J. Earth Sci.*, 48, 857–866.
- 712 Fergusson, C. L., R. A. Henderson, K. J. Lewthwaite, D. Phillips, and I. W. Withnall (2005),
713 Structure of the Early Palaeozoic Cape River Metamorphics, Tasmanides of north
714 Queensland: evaluation of the roles of convergent and extensional tectonics, *Aust. J.*
715 *Earth Sci.*, 52, 261–277.
- 716 Fergusson, C. L., R. A. Henderson, C. M. Fanning, and I. W. Withnall (2007), Detrital zircon
717 ages in Neoproterozoic to Ordovician siliciclastic rocks, northeastern Australia:
718 implications for the tectonic history of the East Gondwana continental margin, *J. Geol.*

- 719 *Soc. London, 164, 215–225.*
- 720 Foden, J., M. Sandiford, J. Dougherty-Page, and I. Williams (1999), Geochemistry and
721 geochronology of the Rathjen Gneiss: implications for the early tectonic evolution of the
722 Delamerian Orogen, *Aust. J. Earth Sci.*, *46*, 377–389.
- 723 Foster, D. (2004), Proterozoic low temperature metamorphism in the Mount Isa Inlier,
724 northwest Queensland, Australia, with particular emphasis on the use of calcic amphibole
725 chemistry as temperature-pressure indicators, Ph.D. thesis, 262 pp., James Cook
726 University, Townsville, Queensland.
- 727 Foster, D. R. W. (in press), An empirical calibration for temperature dependence of Ti
728 substitution in calcic amphiboles in amphibolite, and application to low-pressure, high-
729 temperature amphibolites from the Mount Isa Inlier, northwest Queensland, Australia,
730 *Precambrian Res.*
- 731 Foster, D. A., D. R. Gray, and M. Bucher (1999), Chronology of deformation within the
732 turbidite-dominated Lachlan orogen: implications for the tectonic evolution of eastern
733 Australia and Gondwana, *Tectonics*, *18*, 452–485.
- 734 Foster, D. A., D. R. Gray, and C. Spaggiari (2005), Timing of subduction and exhumation
735 along the Cambrian East Gondwana margin, and the formation of Paleozoic backarc
736 basins, *Geol. Soc. Amer. Bull.*, *117*, 105–116.
- 737 Geological Survey of Queensland (2005), *Geological Site Data*. Department of Natural
738 Resources and Mines, digital data released on CD-ROM (updated annually).
- 739 Gibson, R. L. (1991), Hercynian low-pressure–high-temperature regional metamorphism and
740 subhorizontal foliation development in the Canigou massif, Pyrenees, France—Evidence for
741 crustal extension, *Geology*, *19*, 380–383.
- 742 Glen, R. A. (2005), The Tasmanides of eastern Australia, in *Terrane Processes at the Margins*

- 743 *of Gondwana*, edited by A. P. M. Vaughan, P. T. Leat and R. J. Pankhurst, pp. 23–96,
744 Geol. Soc. London, Spec. Pub. 246.
- 745 Glen, R. A., J. L. Walshe, L. M. Barron, and J. J. Watkins (1998), Ordovician convergent-
746 margin volcanism and tectonism in the Lachlan sector of east Gondwana, *Geology*, *26*,
747 751–754.
- 748 Goodge, J. W., P. Myrow, I. S. Williams, and S. A. Bowring (2002), Age and provenance of
749 the Beardmore Group, Antarctica: constraints on Rodinia supercontinent breakup, *J.*
750 *Geol.*, *110*, 393–406.
- 751 Goodge, J. W., I. S. Williams, and P. Myrow (2004a), Provenance of Neoproterozoic and
752 lower Paleozoic siliciclastic rocks of the central Ross Orogen, Antarctica: Detrital record
753 of rift-, passive- and active-margin sedimentation, *Geol. Soc. Amer. Bull.*, *116*,
754 1253–1279.
- 755 Goodge, J. W., P. Myrow, D. Phillips, C. M. Fanning, and I. S. Williams (2004b), Siliciclastic
756 record of rapid denudation in response to convergent-margin orogenesis, Ross Orogen,
757 Antarctica, in *Detrital thermochronology—Provenance analysis, exhumation, and*
758 *landscape evolution of mountain belts*, edited by M. Bernet and C. Spiegel, pp. 105–126.
759 Geol. Soc. Amer. Spec. Pap. 378.
- 760 Gradstein, F. M., and J. G. Ogg (2004), Geologic Time Scale 2004 – why, how, and where
761 next! *Lethaia*, *37*, 175–181, doi: 10.1080/00241160410006483.
- 762 Haines, P. W., and T. Flöttmann (1998), Delamerian Orogeny and potential foreland
763 sedimentation: a review of age and stratigraphic constraints, *Aust. J. Earth Sci.*, *45*, 559–
764 570.
- 765 Hall, R. (2002), Cenozoic geological and plate tectonic evolution of SE Asia and the SW
766 Pacific: computer-based reconstructions, model and animations, *J. Asian Earth Sci.*, *20*,

- 767 353–431.
- 768 Hammond, R. L. (1986), Large scale structural relationships in the Palaeozoic of northeastern
769 Queensland: melange and mylonite development, and the regional distribution of strain,
770 Ph.D. thesis, 327 pp., James Cook University, Townsville, Queensland.
- 771 Hand, M., J. Mawby, P. Kinny, and J. Foden (1999), U–Pb ages from the Harts Range, central
772 Australia: evidence for early Ordovician extension and constraints on Carboniferous
773 metamorphism, *J. Geol. Soc. London*, *156*, 715–730.
- 774 Harris, L. B., H. A. Koyi, and H. Fossen (2002), Mechanisms for folding of high-grade rocks
775 in extensional tectonic settings, *Earth-Sci. Rev.*, *59*, 163–210.
- 776 Henderson, R. A. (1980), Structural outline and summary geological history for northeastern
777 Australia, in *The Geology and Geophysics of Northeastern Australia*, edited by R. A.
778 Henderson and P. J. Stephenson, pp. 1–26, Geol. Soc. Aust., Queensland Division.
- 779 Henderson, R. A. (1983), Early Ordovician faunas from the Mount Windsor Subprovince,
780 northeastern Queensland, *Mem. Austral. Assoc. Palaeont.*, *1*, 145–175.
- 781 Henderson, R. A. (1986), Geology of the Mt Windsor Subprovince – a Lower Palaeozoic
782 volcano-sedimentary terrane in the northern Tasman Orogenic Zone, *Aust. J. Earth Sci.*, *33*,
783 343–364.
- 784 Holland, T. and J. Blundy (1994), Non-ideal interactions in calcic amphiboles and their
785 bearing on amphibole-plagioclase thermometry, *Contrib. Mineral. Petrol.*, *116*, 433–447.
- 786 Hoskin, P. W. O. (2000), Patterns of chaos: fractal statistics and the oscillatory chemistry of
787 zircon, *Geochim. Cosmochim. Acta*, *64*, 1905–1923.
- 788 Hutton, L. J., J. J. Draper, I. P. Rienks, I. W. Withnall, and J. Knutson (1997), *Charters Towers*
789 *region*, in *North Queensland Geology*, edited by J. H. C. Bain and J. J. Draper J. J., pp.
790 165–224,. Australian Geological Survey Organisation Bulletin 240 and Queensland

- 791 Geology 9.
- 792 Hyndman, R. D., C. A. Currie, and S. P. Mazzotti (2005), Subduction zone backarcs, mobile
793 belts, and orogenic heat, *GSA Today*, 15, 4–10.
- 794 Lister, G. S., G. Banga, and A. Feenstra (1984), Metamorphic core complexes of Cordilleran
795 type in the Cyclades, Aegean Sea, Greece, *Geology*, 12, 221–225.
- 796 Ludwig, K. R. (1999), *User's manual for Isoplot/Ex, Version 2.10, A geochronological toolkit*
797 *for Microsoft Excel*, Berkeley Geochronology Center Special Publication 1, 47 pp., 2455
798 Ridge Road, Berkeley, CA 94709, USA.
- 799 Ludwig, K. R. (2000), *SQUID 1.00, A User's Manual*, Berkeley Geochronology Center
800 Special Publication 2, 17 pp., 2455 Ridge Road, Berkeley, CA 94709, USA.
- 801 McDougall, I., and T. M. Harrison (Eds.) (1999), *Geochronology and thermochronology by*
802 *the $^{40}\text{Ar}/^{39}\text{Ar}$ method*, 2nd ed., 269 pp., Oxford Univ. Press, New York.
- 803 McKenzie, D. (1978) Some remarks on the origin of sedimentary basins, *Earth Planet. Sci.*
804 *Lett.*, 40, 25–32.
- 805 Miller, J. McL., D. Phillips, C. J. L. Wilson, and L. J. Dugdale (2005), Evolution of a
806 reworked Orogenic Zone: the boundary between the Delamerian and Lachlan Fold Belts,
807 southeastern Australia, *Aust. J. Earth Sci.*, 52, 921–940.
- 808 Murray, C. G., and A. G. Kirkegaard (1978), The Thomson Orogen of the Tasman Orogenic
809 Zone, *Tectonophysics*, 48, 299–325.
- 810 Nishiya, T., T. Watanabe, K. Yokoyama, and Y. Kuramoto (2003), New isotopic constraints
811 on the age of the Halls Reward Metamorphics, North Queensland, Australia: Delamerian
812 metamorphic ages and Grenville detrital zircons, *Gondwana Res.*, 6, 241–249.
- 813 Paces, J. B., and J. D. Miller (1993), Precise U–Pb ages of Duluth Complex and related mafic
814 intrusions, northeastern Minnesota: Geochronological insights to physical, petrogenetic,

- 815 paleomagnetic, and tectonomagmatic processes associated with the 1.1 Ga Midcontinent
816 Rift System, *J. Geophys. Res.*, *98*, 13997–14013.
- 817 Packham, G. H., J. B. Keene, and L. M. Barron (2003), Middle to early Late Ordovician
818 hydrothermal veining in the Molong Volcanic Belt, northeastern Lachlan Fold Belt:
819 sedimentological evidence, *Aust. J. Earth Sci.*, *50*, 257–269.
- 820 Pavlis, T. L., and V. B. Sisson (1993), Mid-Cretaceous extensional tectonics of the Yukon-
821 Tanana terrane, Trans-Alaska Crustal Transect (TACT), east-central Alaska, *Tectonics*,
822 *12*(1), 103–122.
- 823 Pisarevsky, S. A., M. T. D. Wingate, C. McA. Powell, S. Johnson, and D. A. D. Evans (2003),
824 Models of Rodinia assembly and fragmentation, in *Proterozoic East Gondwana:*
825 *Supercontinent Assembly and Breakup*, edited by M. Yoshida, B. F. Windley and S.
826 Dasgupta, pp. 35–55, Geol. Soc. London, Spec. Publ. 206.
- 827 Preiss, W. V. (2000), The Adelaide Geosyncline of South Australia and its significance in
828 Neoproterozoic continental reconstruction, *Precambrian Res.*, *100*, 21–63.
- 829 Ramsay, J. G., M. Casey, and R. Kligfield (1983), Role of shear in development of the
830 Helvetic fold-thrust belt of Switzerland, *Geology*, *11*, 439–442.
- 831 Reid, A. J., C. J. L. Wilson, D. Phillips and S. Liu (2005), Triassic exhumation across the
832 Yidun Arc, eastern Tibetan Plateau: tectonic implications from $^{40}\text{Ar}/^{39}\text{Ar}$
833 thermochronology, *Tectonophysics*, *398*, 45–66.
- 834 Richards, S. W., and W. J. Collins (2002), The Cooma Metamorphic Complex, a low-*P*, high-
835 *T* (*LPHT*) regional aureole beneath the Murrumbidgee Batholith, *J. Metamorphic Geol.*,
836 *20*, 119–134.
- 837 Ring, U., and P. W. Layer (2003), High-pressure metamorphism in the Aegean, eastern
838 Mediterranean: underplating and exhumation from the Late Cretaceous until the Miocene to

- 839 Recent above retreating Hellenic subduction zone, *Tectonics*, 22(3),
840 doi:10.1029/2001TC001350:1–23.
- 841 Spear, F. S. (1995), *Metamorphic phase equilibria and pressure-temperature-time paths*, 799
842 pp., Mineralogical Society of America Monograph, Washington.
- 843 Roddick, J. C. (1983), High precision inter-calibration of ^{40}Ar - ^{39}Ar standards, *Geochim.*
844 *Cosmochim. Acta*, 47, 887–898.
- 845 Sandiford, M. (1989), Horizontal structures in granulite terrains: a record of mountain
846 building or mountain collapse? *Geology*, 17, 449–452.
- 847 Spaggiari, C. V., D. R. Gray, and D. A. Foster (2003), Tethyan- and Cordilleran-type
848 ophiolites of eastern Australia: implications for the evolution of the Tasmanides, in
849 *Ophiolites in Earth History*, edited by Y. Dilek and P. T. Robinson, pp. 517–539, Geol.
850 Soc. London, Spec. Pub. 218.
- 851 Squire, R., and C. J. L. Wilson (2005), Interaction between collisional orogenesis and
852 convergent margin processes: evolution of the Cambrian proto-Pacific margin of East
853 Gondwana, *J. Geol. Soc. London*, 162, 749–761.
- 854 Steiger, R. H., and E. Jäger (1977), Subcommittee on geochronology: Convention on the use
855 of decay constants in geo- and cosmochronology, *Earth Planet. Sci. Lett.*, 36, 359–362.
- 856 Stern, R. J. (2002), Subduction zones, *Rev. Geophys.*, 40(4), doi:10.1029/2001RG000108.
- 857 Stolz, A. J. (1995), Geochemistry of the Mount Windsor Volcanics: implications for the
858 tectonic setting of Cambro-Ordovician volcanic-hosted massive sulphide mineralisation
859 in northeastern Australia, *Econ. Geol.*, 90, 1080–1097.
- 860 Stump, E. (1995), *The Ross Orogen of the Transantarctic Mountains*, 284 pp., Cambridge
861 University Press, Cambridge, UK.
- 862 Thompson, A. B., K. Schulmann, J. Jezek, and V. Tolar (2001), Thermally softened

- 863 continental extension zones (arcs and rifts) as precursors to thickened orogenic belts,
864 *Tectonophysics*, 332, 115–141.
- 865 Turner, G., J. C. Huneke, F. A. Podosek and G. J. Wasserburg (1971), ^{40}Ar - ^{39}Ar ages and
866 cosmic ray exposure ages for Apollo 14 samples, *Earth Planet. Sci. Lett.*, 12, 19–35.
- 867 Vandenberg, A. H. M., C. E. Willman, S. Maher, B. A. Simons, R. A. Cayley, D. H. Taylor, V.
868 J. Morand, D. H. Moore and A. Radojkovic (2000), *The Tasman Fold Belt System in*
869 *Victoria. Geology and mineralisation of Proterozoic to Carboniferous rocks*, 462 pp.,
870 Geological Survey of Victoria Special Publication, Melbourne, Australia.
- 871 Williams, I. S. (1998), U-Th-Pb Geochronology by Ion Microprobe, in *Applications of*
872 *microanalytical techniques to understanding mineralizing processes*, edited by M. A.,
873 McKibben, W. C. Shanks III and W. I. Ridley, pp. 1–35, *Rev. Econ. Geol.* 7.
- 874 Withnall, I. W., and T. P. T. McLennan (1991), *Geology of the northern part of the Lolworth-*
875 *Ravenswood Province*, Record 1991/12, 56 pp., Department of Resources Industries,
876 Queensland.
- 877 Withnall, I. W., and S. C. Lang (Eds.) (1993), *Geology of the Broken River Province, north*
878 *Queensland*, Queensland Geology 4, 292 pp., Department of Minerals and Energy,
879 Queensland.
- 880 Withnall, I. W., P. R. Blake, S. B. S. Crouch, K. Tenison Woods, M. A. Hayward, J. S. Lam, P.
881 Garrad, and I. D. Rees (1995), *Geology of the southern part of the Anakie Inlier, central*
882 *Queensland*, Queensland Geology 7, 245 pp., Department of Minerals and Energy,
883 Queensland.
- 884 Withnall, I. W., S. D. Golding, I. D. Rees, and S. K. Dobos (1996), K-Ar dating of the Anakie
885 Metamorphic Group: evidence for an extension of the Delamerian Orogeny into central
886 Queensland, *Aust. J. Earth Sci.*, 43, 567–572.

887 Withnall, I. W., L. J. Hutton, and R. K. J Blight (2003), *North Queensland Gold and Base*
888 *Metal Study Stage 2 – Charters Towers GIS*. Geological Survey of Queensland,
889 Department of Natural Resources and Mines, digital data (including explanatory notes)
890 released on CD-ROM.

891 Wysoczanski, R. J., and A. H. Allibone (2004), Age, correlation and provenance of the
892 Neoproterozoic Skelton Group, Antarctica: Grenville age detritus on the margin of East
893 Antarctica, *J. Geol.*, *112*, 401–416.

894

895

896 **Figure Captions**

897

898 **Figure 1.** (a) Extent of the Ross-Delamerian orogenic belt in East Gondwana. (b) Orogenic
899 belts and the Precambrian craton in eastern Australia (Mesozoic and younger cover not shown).
900 Tasman Orogenic Zone includes the Lachlan Fold Belt, New England Fold Belt, Thomson Fold
901 Belt (incorporating the Anakie Inlier, Charters Towers Province = CTP, Greenvale Province =
902 GP), Hodgkinson-Broken River Fold Belt and eastern part of the Adelaide Fold Belt.

903

904 **Figure 2.** Regional map of Charters Towers Province. The Broken River Fold Belt
905 includes the Graveyard Creek Subprovince in the west and the Camel Creek Subprovince in the
906 east. Location of Figure 3.

907

908 **Figure 3.** Map of the Argentine Metamorphics in the main area of exposure around the
909 locality of Argentine [after *Withnall and McLennan*, 1991; *Withnall et al.*, 2003] but with some
910 revision including greater mapped extent of higher grade unit (Amg) into Middle and Stockyard

911 Creeks.

912

913 **Figure 4.** Cross sections through the Argentine Metamorphics (for location see Figure 3).

914 Key to symbols: Amo = orthogneiss, Amsa = schist/amphibolite, Amp = phyllite, Amg =

915 paragneiss, Ams = schist/semischist, short dashed line pattern = mafic schist/amphibolite.

916

917 **Figure 5.** Lower hemisphere equal area stereographic projections of structural data from

918 the Argentine Metamorphics. Number of measurements shown for each stereonet on lower

919 left side. Contour intervals 1-2-4-8-(16)% per 1% area for contoured plots. (a) Poles to S_2

920 foliation, β -axis $45^\circ/180^\circ$, mean $45^\circ/184^\circ$. (b) L_2 lineations, mean $41^\circ/145^\circ$, girdle $41^\circ/134^\circ$.

921 (c) L_m mineral lineation, mean $61^\circ/137^\circ$. (d) S_3 foliation, mean $29^\circ/173^\circ$. (e) F_3 axes, mean

922 $19^\circ/107^\circ$. (f) S_4 foliation, mean $86^\circ/273^\circ$. (g) F_4 axes, girdle $87^\circ/095^\circ$. (h) Cattle Creek Dome,

923 S_2 foliation, mean $15^\circ/133^\circ$.

924

925 **Figure 6.** (a) Steeply dipping S_2 crenulation cleavage in low-grade phyllite of the

926 Argentine Metamorphics (0385871 7863949 Ewan 8059 1:100 000 sheet). (b) Layering with

927 isoclinal folds subparallel to S_2 foliation in low-grade quartzite (0410437 7850666 Rollingstone

928 8159 1:100 000 sheet). (c) Multiply deformed high-grade psammitic gneiss (0413357 7852019

929 Rollingstone 8159 1:100 000 sheet). (d) Flat-lying S_2 foliation in quartz-mica phyllonite with

930 quartz veins boudinaged by low-angle shear bands indicating top to the north shearing (0420236

931 7853946 Rollingstone 8159 1:100 000 sheet).

932

933 **Figure 7.** Photomicrograph of foliation defined by hornblende in sample AM89

934 (amphibolite).

935

936 **Figure 8.** Representative CL images of zircon grains analyzed by SHRIMP, (a) sample
937 IWAM162D (felsic clast in mafic breccia), (b) sample HR1 (foliated Mingela Granodiorite),
938 and (c) AM77 (massive granodiorite).

939

940 **Figure 9.** (a) U–Pb analyses and ages for sample IWAM162D (felsic clast in mafic
941 breccia) from the Argentine Metamorphics (0393359 7861812 Ewan (8059) 1:100 000 sheet).
942 Logarithmic Tera-Wasserburg diagram and histogram of U–Pb zircon ages with
943 superimposed probability distribution. In histograms the shaded columns represent data used
944 in age calculation (see text). (b) U–Pb analyses and ages for sample HR1 (foliated Mingela
945 Granodiorite) (0431951 7843606 Dotswood (8158) 1:100 000 sheet). Logarithmic Tera-
946 Wasserburg diagram, detailed Logarithmic Tera-Wasserburg diagram and histogram of U–Pb
947 zircon ages with superimposed probability distribution. (c) U–Pb analyses and ages for
948 sample AM77 (massive granodiorite) from a vein cross-cutting the Argentine Metamorphics
949 (0422451 7850414 Rollingstone (8159) 1:100 000 sheet). Logarithmic Tera-Wasserburg
950 diagram and histogram of U–Pb zircon ages with superimposed probability distribution.

951

952 **Figure 10.** $^{40}\text{Ar}/^{39}\text{Ar}$ plateau for sample AM89 (amphibolite).

953

954 **Figure 11.** Time-space plot with comparison of critical data (U–Pb zircon ages, $^{40}\text{Ar}/^{39}\text{Ar}$
955 ages and stratigraphic ranges) from the Argentine Metamorphics [*this paper*] and Charters
956 Towers Province [Seventy Mile Range Group, *Henderson*, 1983, 1986; Macrossan Igneous
957 Province, range 507–455 Ma shown of U–Pb zircon ages, *Hutton et al.*, 1997] with other sectors
958 of the Ross-Delamerian orogenic belt along the Pacific margin of East Gondwana including the

959 Adelaide Fold Belt of southeastern Australia – SG = Summerfield Granodiorite – 486 ± 6 Ma,
 960 RGD = Reedy Creek diorite – 487 ± 2 Ma, CWG = Cape Willoughby Granite – 508 ± 7 Ma, HS
 961 = tuff from the Heathersdale Shale – 526 ± 4 Ma [*Haines and Flöttmann, 1998*], RG = Rathjen
 962 Gneiss – 514 ± 5 Ma, [*Foden et al., 1999; Preiss, 2000*], the outboard Macquarie arc of the
 963 Lachlan Fold Belt – U-Pb ages on monzodiorites – 484 ± 3 Ma and 451 ± 4 Ma, [*Butera et al.,*
 964 2001] with major episodes of sedimentation/volcanism from *Packham et al. [2003]*, Middle to
 965 Late Cambrian extensional island arc and backarc basement of the southern Lachlan Fold Belt
 966 [*VandenBerg et al., 2000; Spaggiari et al., 2003*], Tasmania – FC = Forth Complex – 512 ± 5
 967 Ma, HRC = Heazlewood River Complex – 515 ± 7 Ma, FMC = Franklin Metamorphic Complex
 968 – 508 ± 8 Ma, extensional episode with Mt Read Volcanics and $^{40}\text{Ar}/^{39}\text{Ar}$ ages of metamorphic
 969 cooling at 507–508 Ma [*Foster et al., 2005* and references therein], Northern Victoria Land –
 970 $^{40}\text{Ar}/^{39}\text{Ar}$ ages 500–460 Ma with peak of Granite Harbor intrusives at 480 Ma [*Dallmeyer and*
 971 *Wright, 1992; Stump, 1995*], Southern Victoria Land – U-Pb ages for gneissic and weakly
 972 foliated granites – 531 ± 10 Ma, 516 ± 10 Ma, 505 ± 9 Ma, 502 ± 9 Ma, 499 ± 6 Ma [*Allibone*
 973 *and Wysoczanski, 2002*], U-Pb ages 505–480 Ma from metamorphic rims on zircons
 974 [*Wysoczanski and Allibone, 2004*], the Central Transantarctic Mountains – youngest detrital
 975 zircon ages – 505–495 Ma, youngest detrital mica ages – 504 Ma, 510 Ma, 516 Ma and 518 Ma
 976 [*Goodge et al., 2002, 2004a, b*]. Timescale after *Gradstein and Ogg [2004]*.

977

978 **Figure 12.** Schematic cross section for part of the Charters Towers Province towards the
 979 end of extensional deformation at ~ 460 Ma. The upper crust was dominated by the Seventy
 980 Mile Range Group which formed by sedimentation and volcanic activity in an extensional
 981 setting. Extension was accommodated in the upper crust by subsidence, deposition, shallow
 982 intrusions and some syndepositional faulting [*Henderson, 1986; Berry et al., 1992*]. In the

983 middle to lower crust extension was accommodated by pure shear [McKenzie, 1978] with
984 widespread development of flat-lying foliation and associated recumbent folds (not shown).
985 Uplift of metamorphic rocks to the surface was a result of younger extensional and contractional
986 deformation that affected in the region in the Early Silurian and Late Devonian to Late
987 Carboniferous [Henderson, 1980].

988

989 **Figure 13.** Reconstructions of the active Pacific margin of Gondwana. Regions with
990 extensional tectonics shown by diverging arrows; regions with contractional deformation are
991 used to infer the location of continental margin subduction zones. For 520–500 Ma the location
992 of subduction zones in the juvenile arc/island arc region of southeastern Australia is not shown
993 as their location and dip is unknown. For 480 Ma and 460 Ma the Larapintine Seaway is a
994 shallow sea that extends across Australia to the Pacific Ocean in the east. Subduction is shown
995 dying out from south to north although it is likely that outboard subduction zones existed in the
996 Pacific near East Antarctica and are obscured in West Antarctica. For 460 Ma the subduction
997 zone in southeastern Australia reflects the development of several microplates and subduction
998 zones outlined by Foster *et al.* [1999].

999

1000

1001 **Tables**

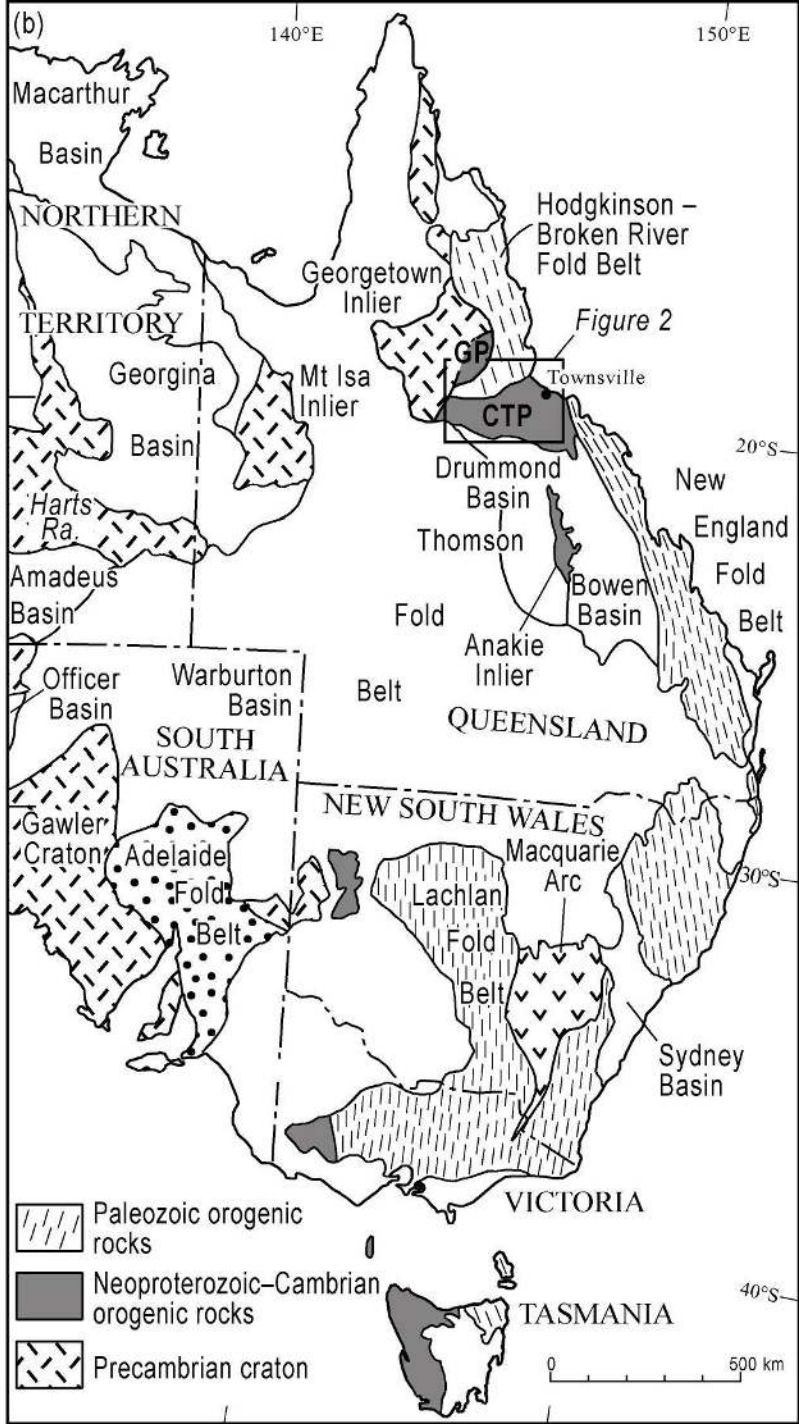
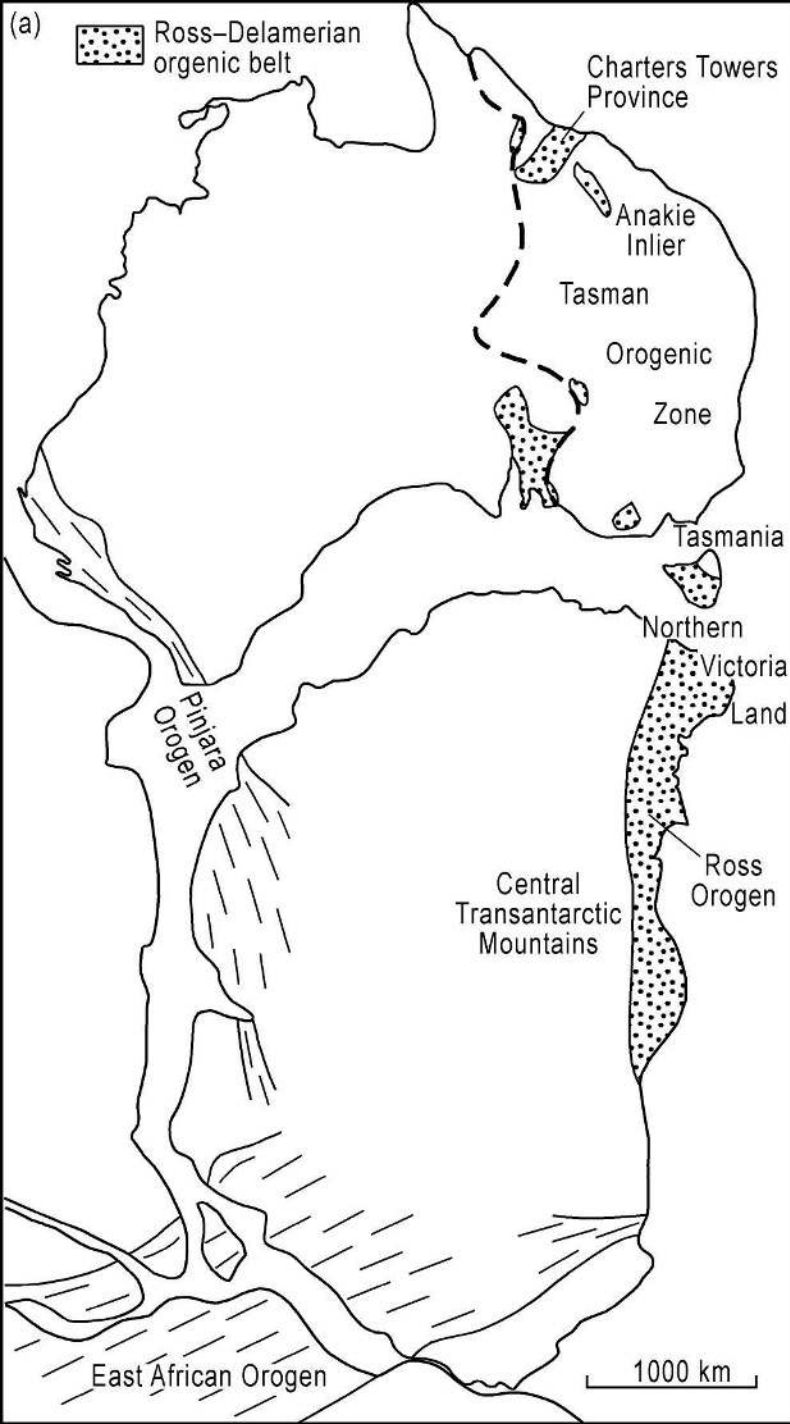
1002

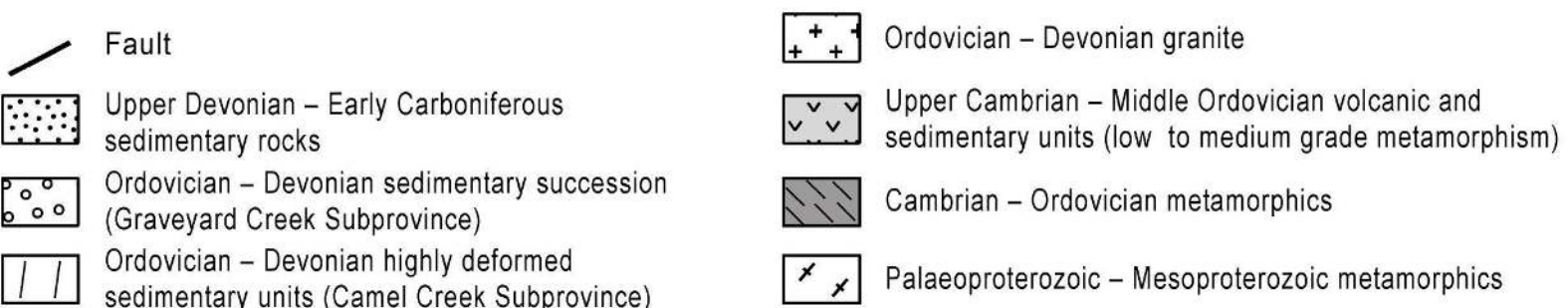
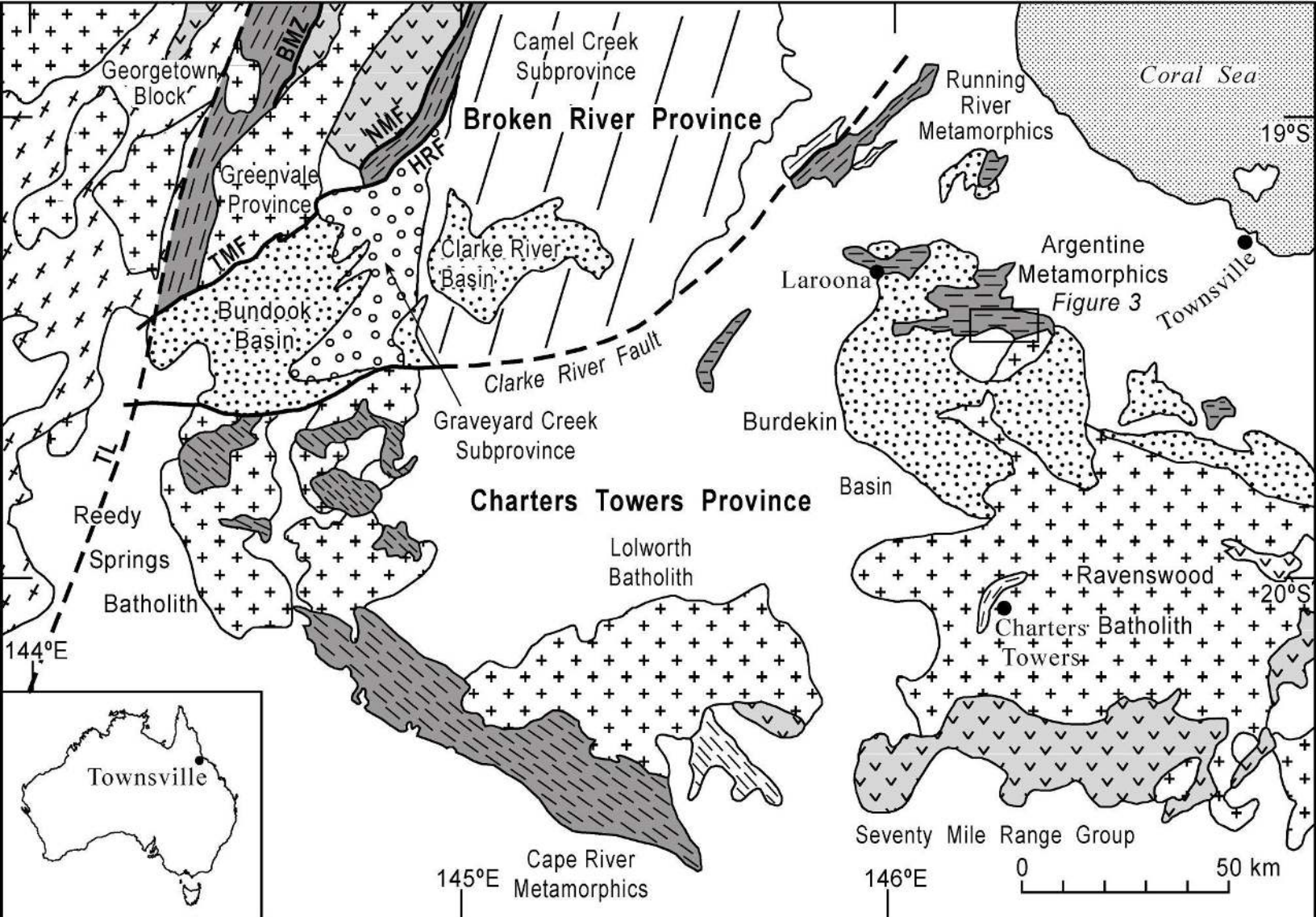
1003 **Table 1.** Deformations in the Argentine Metamorphics.

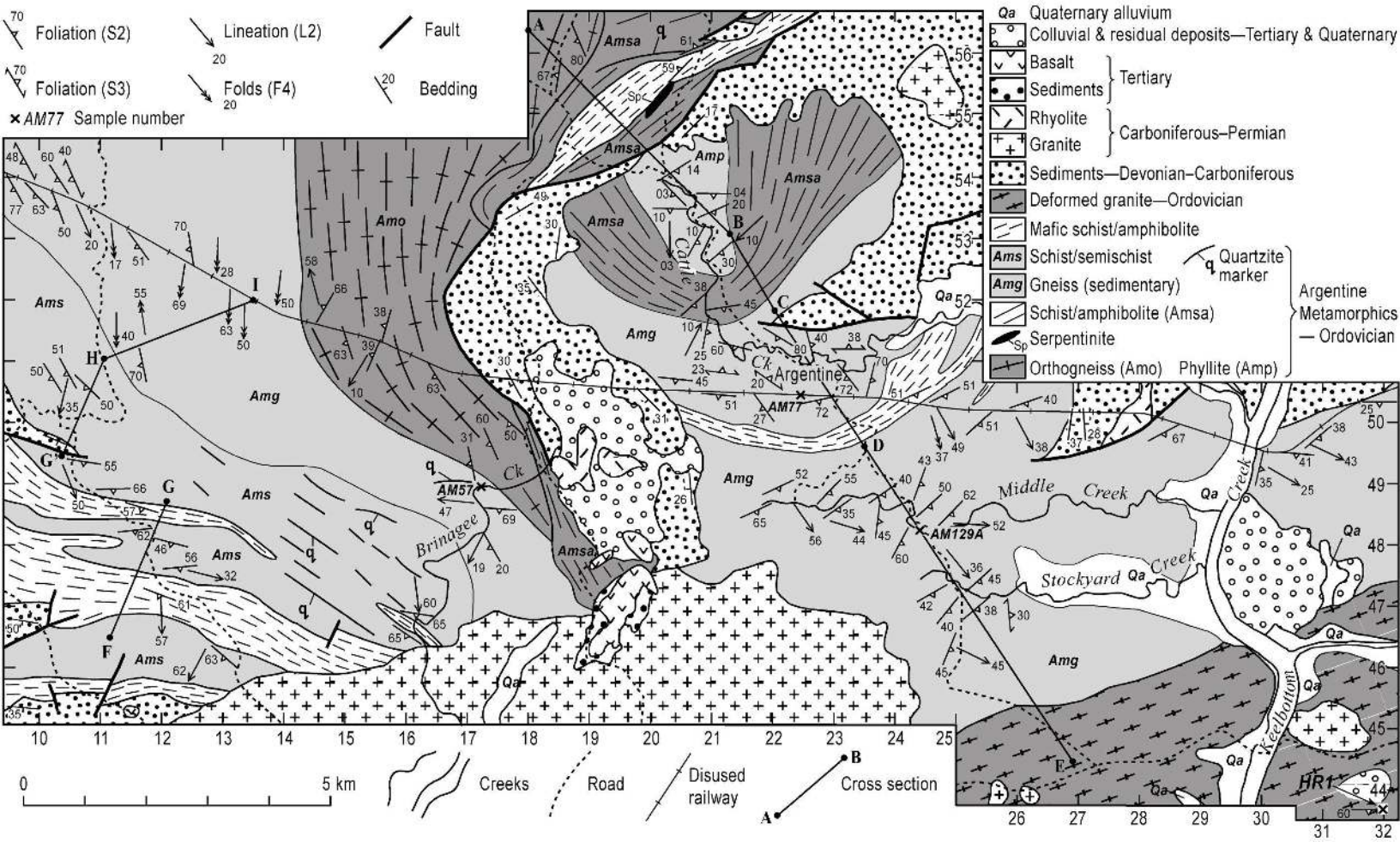
1004

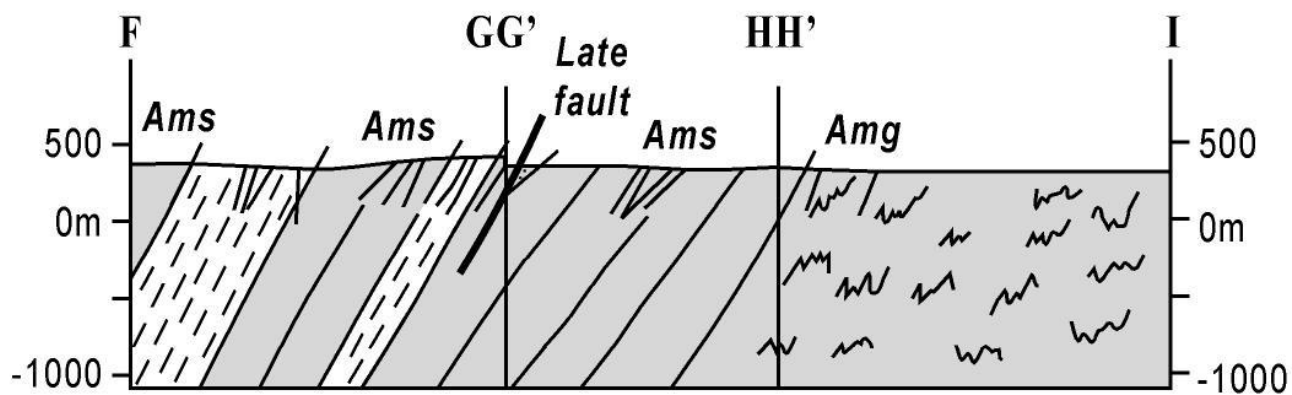
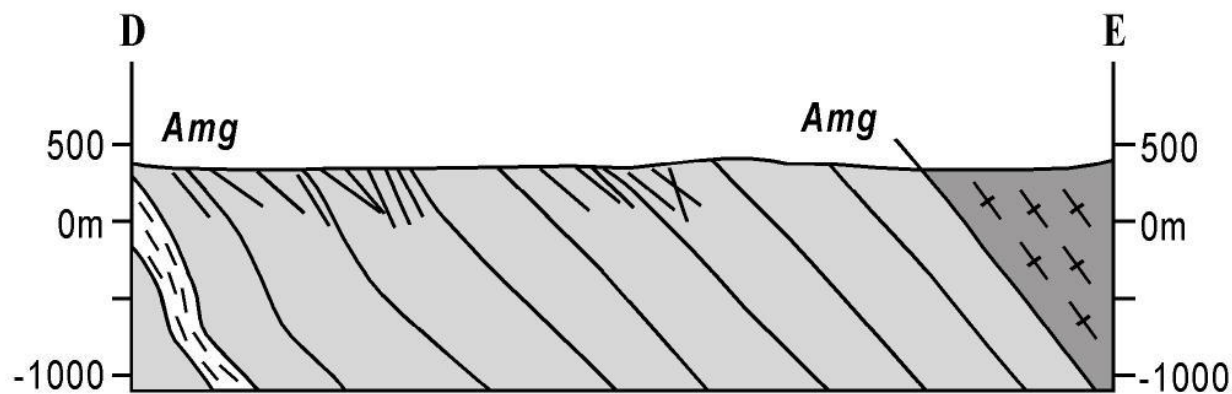
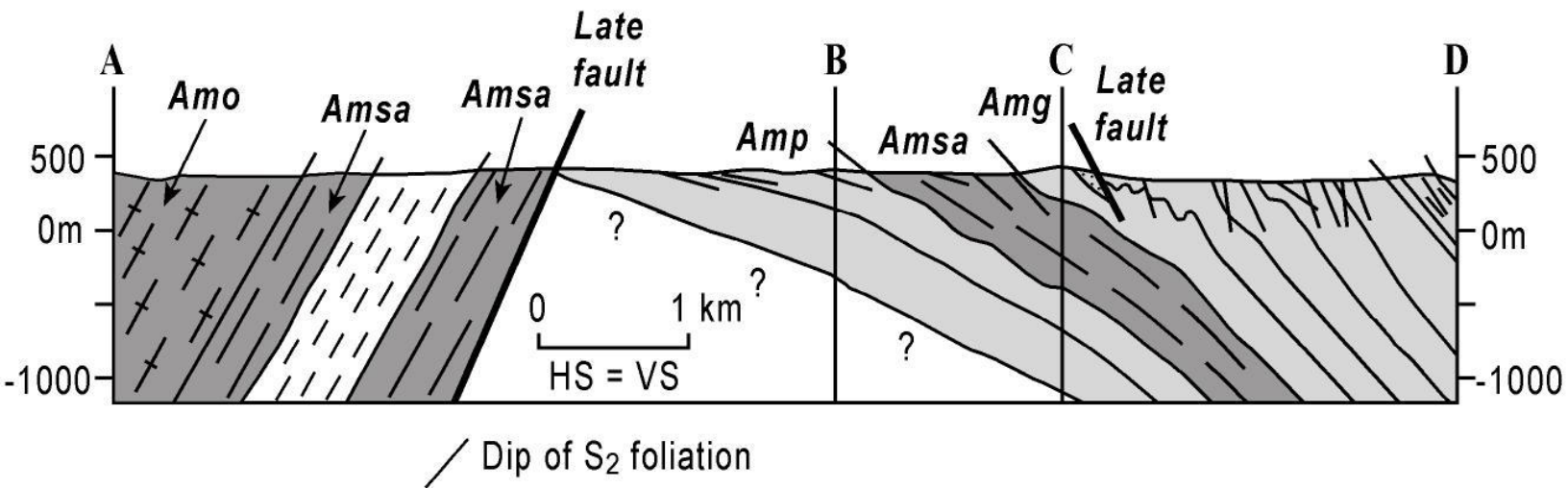
1005 **Table 2.** Temperatures calculated using the titanium oxide thermometer of Foster [in
1006 press].

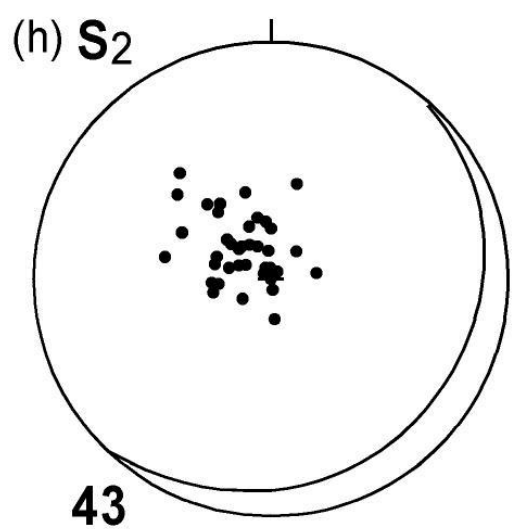
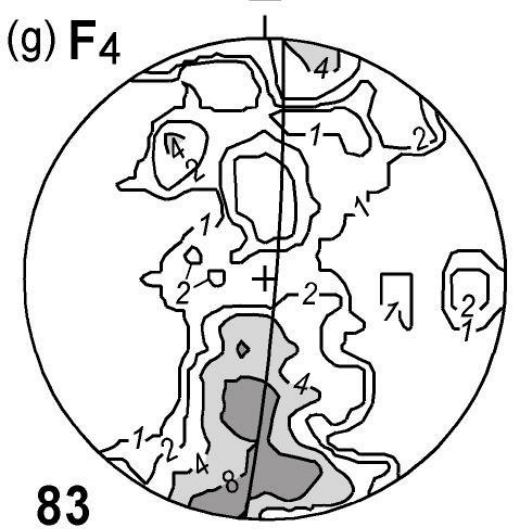
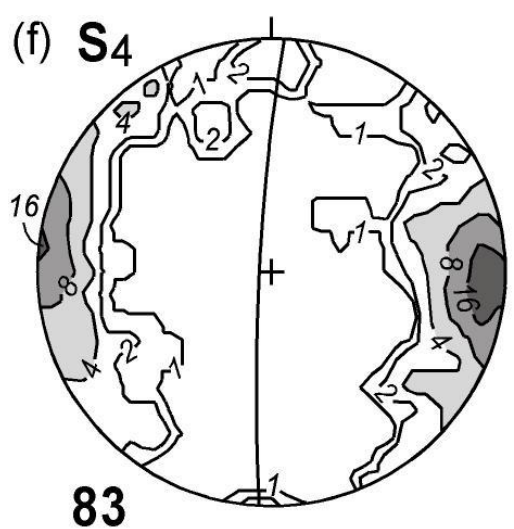
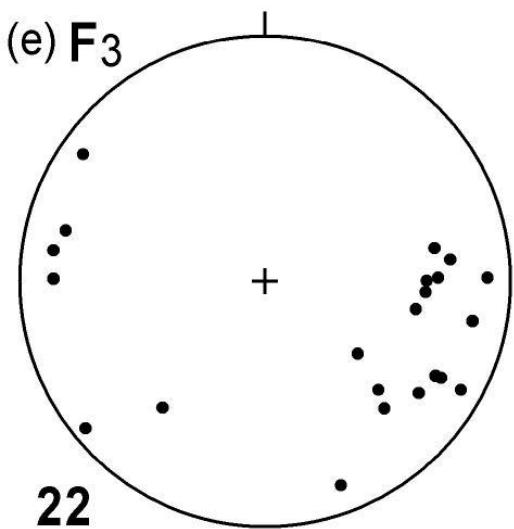
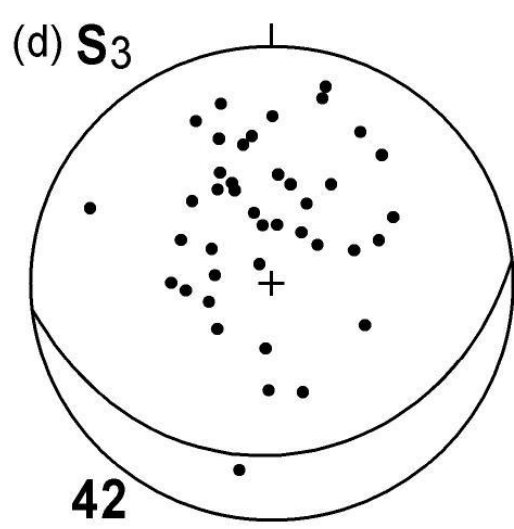
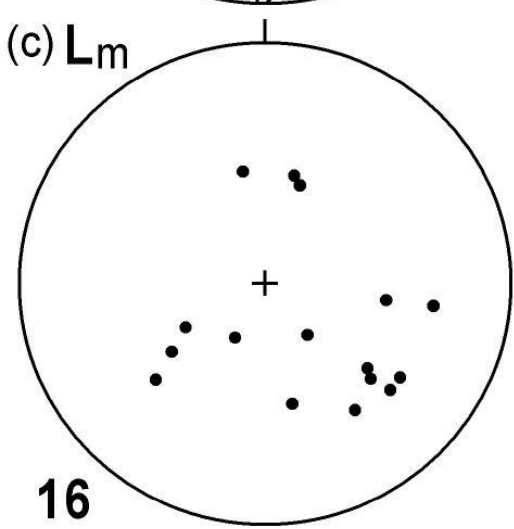
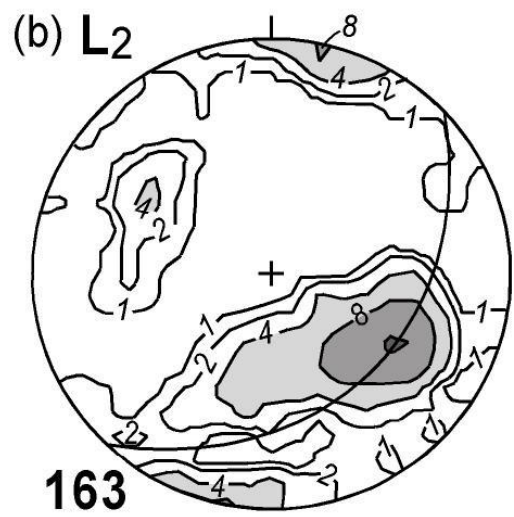
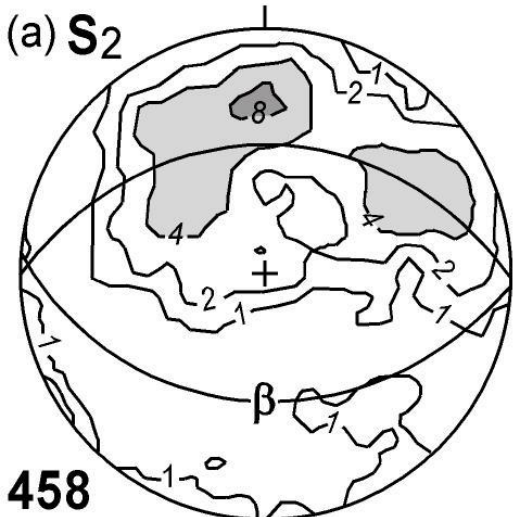
- 1007 **Table 3.** Summary of SHRIMP U-Pb zircon results for sample IWAM162D.
1008
- 1009 **Table 4.** Summary of SHRIMP U-Pb zircon results for sample HR1.
1010
- 1011 **Table 5.** Summary of SHRIMP U-Pb zircon results for sample AM77.
1012
- 1013 **Table 6.** $^{40}\text{Ar}/^{39}\text{Ar}$ step-heating analytical results for sample AM89 (amphibolite).
1014
- 1015 **Supplementary Data**
- 1016 Supplementary Data Table 1. Supplementary electron microprobe analytical data.
- 1017 Supplementary Data Table 2. Calculated geothermometry values (degrees centigrade).

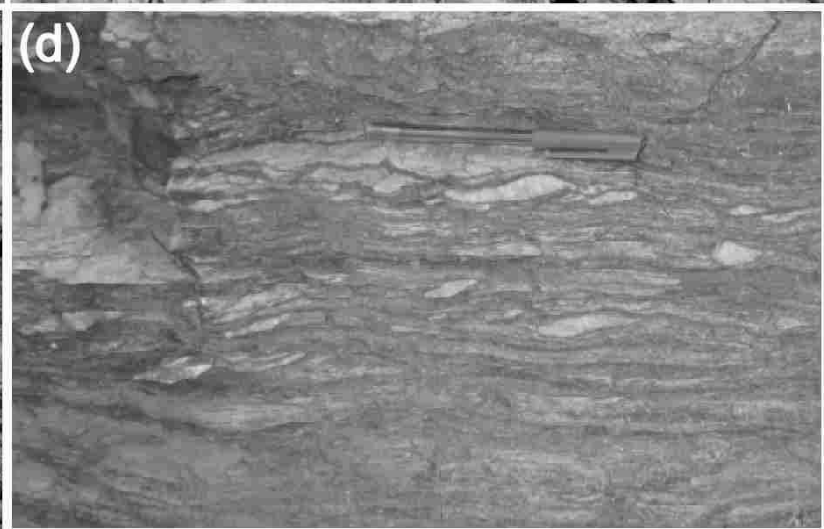
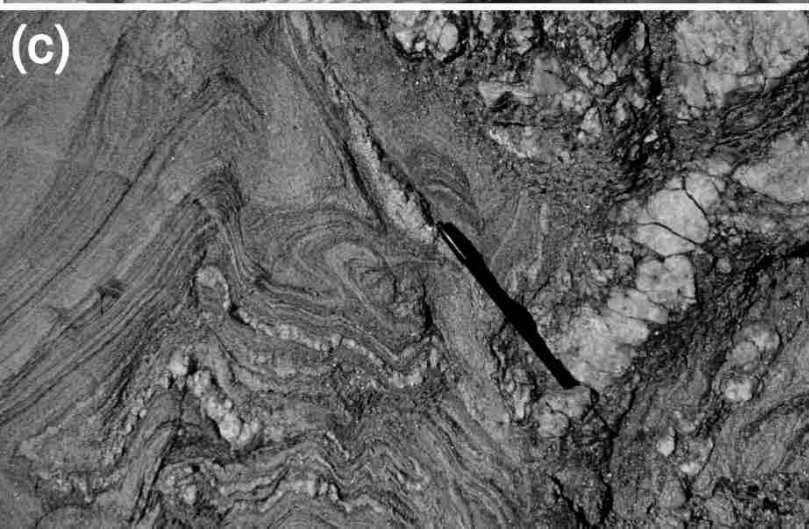


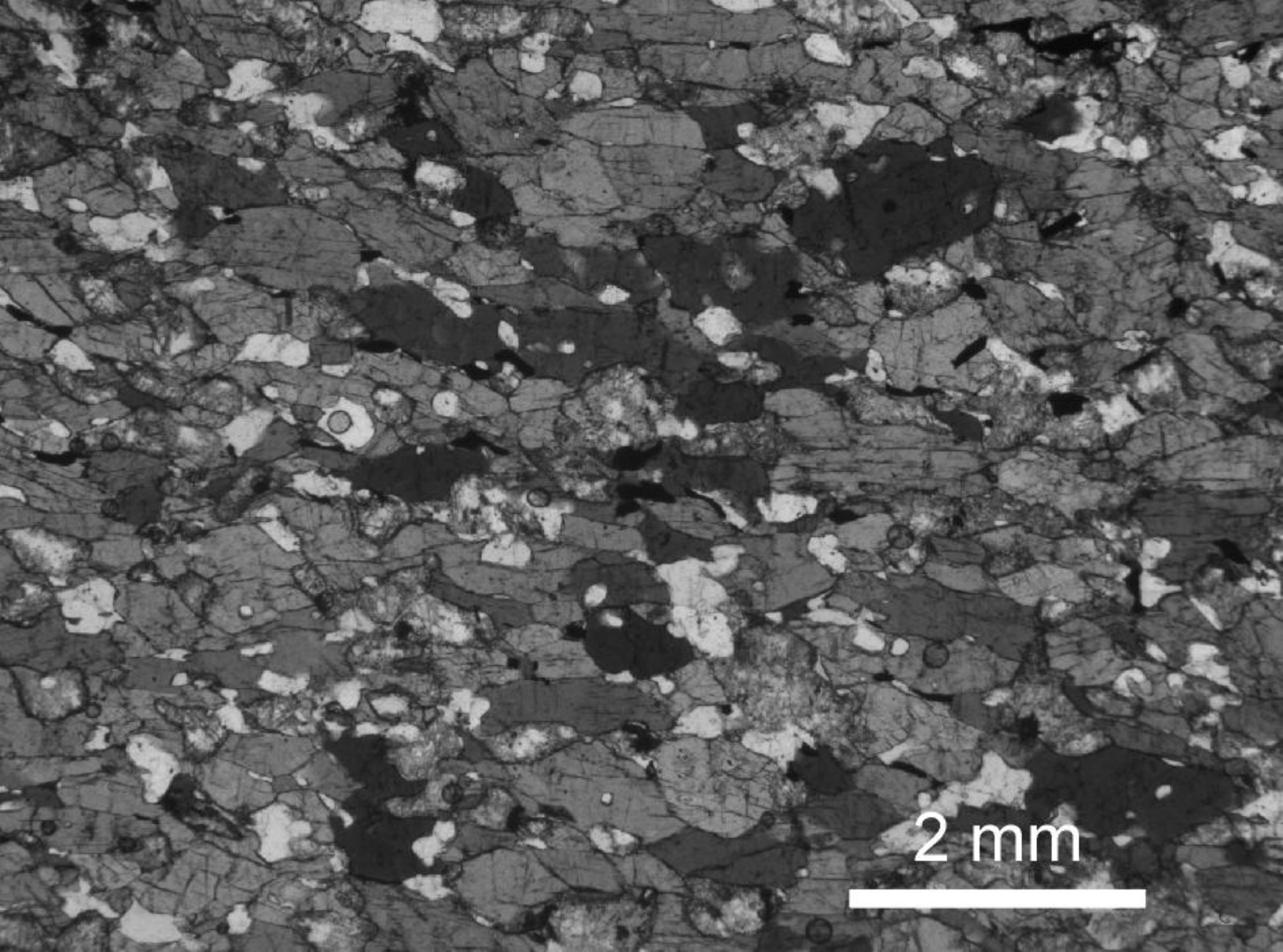






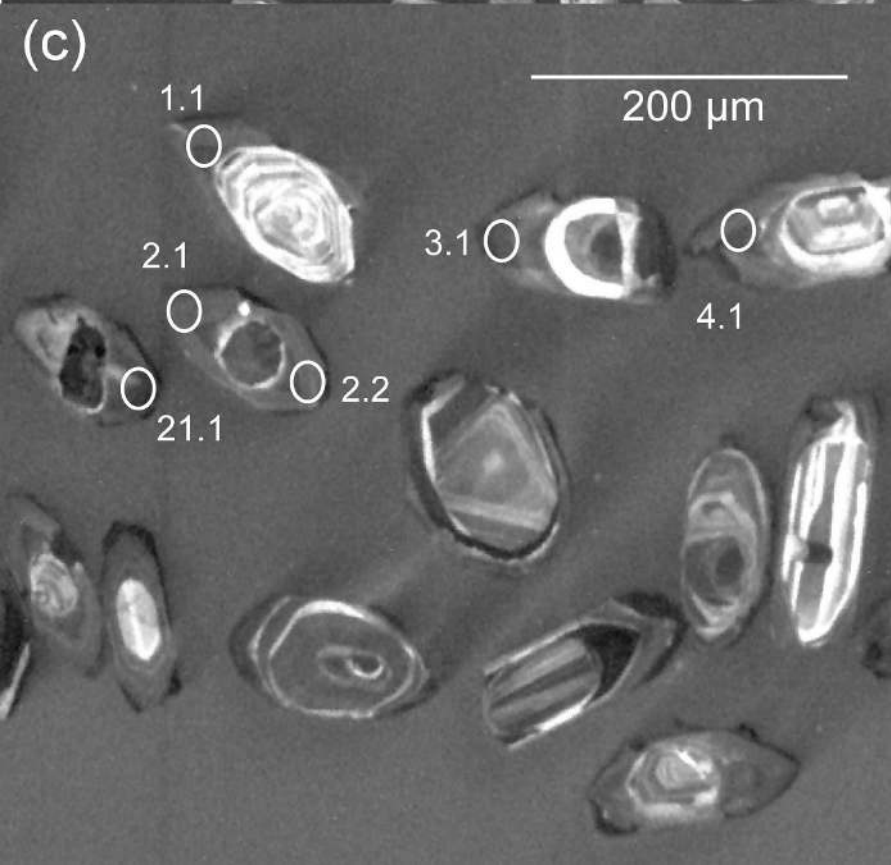
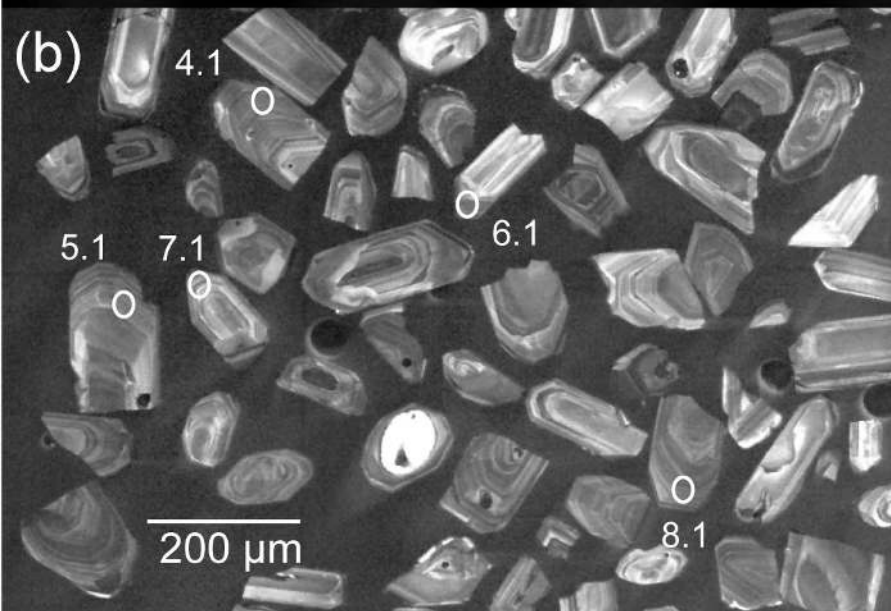
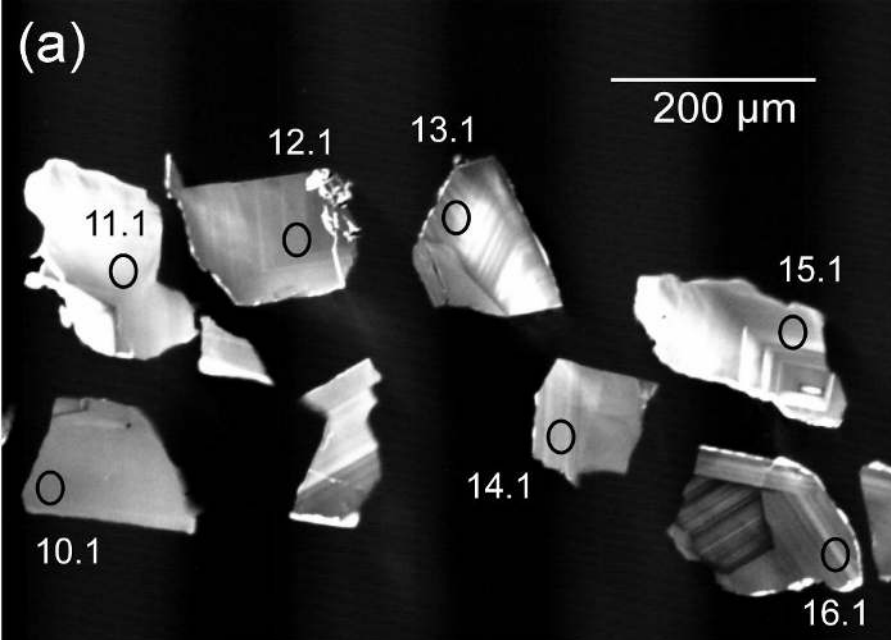


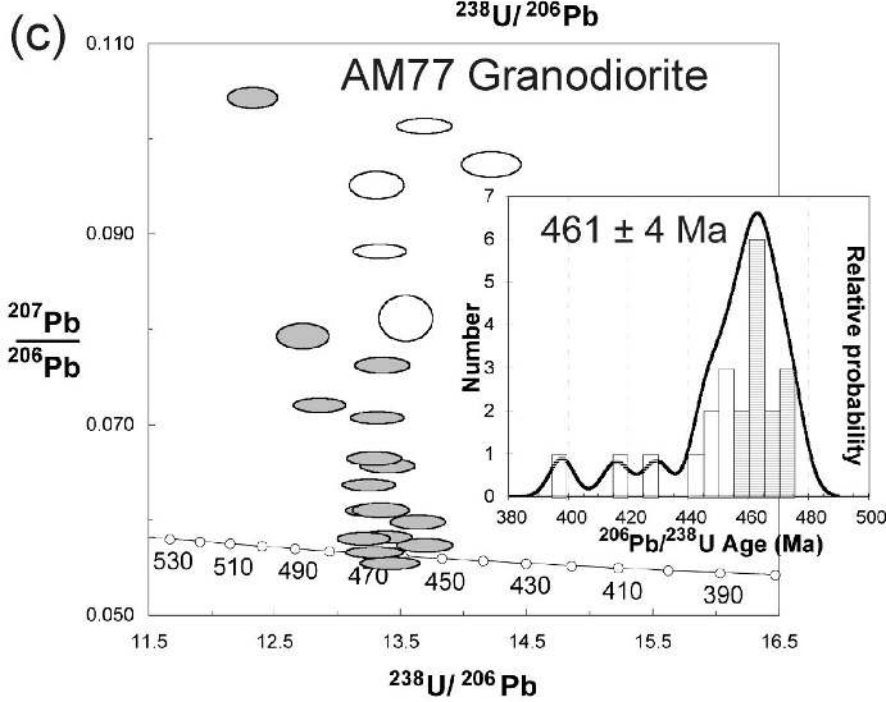
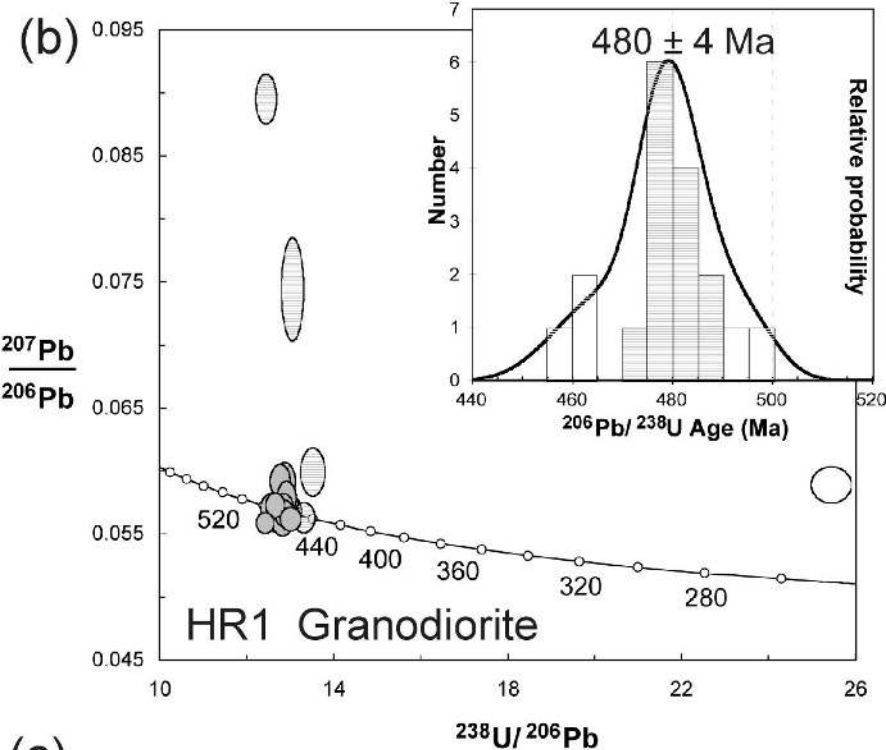
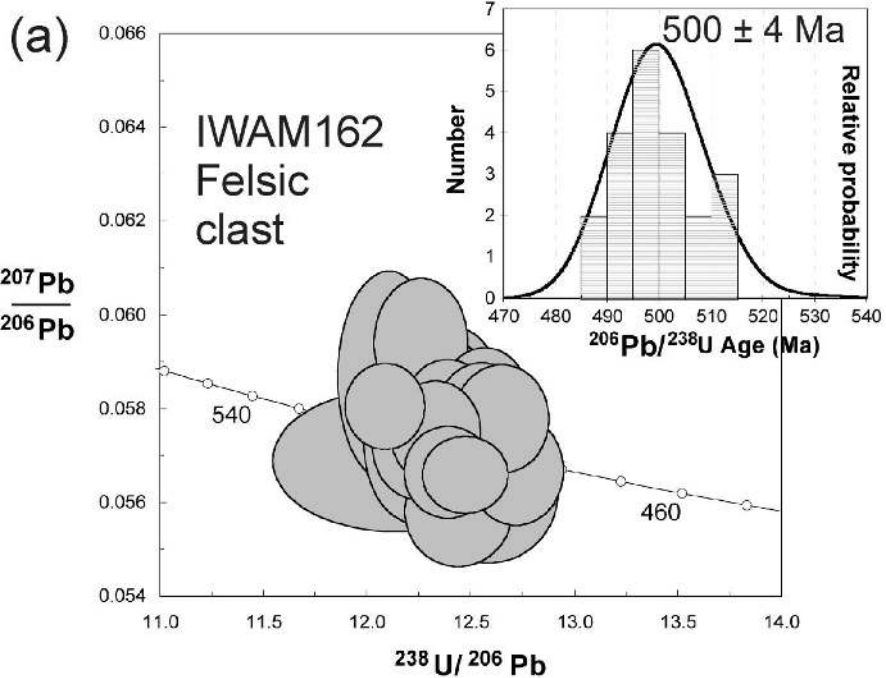


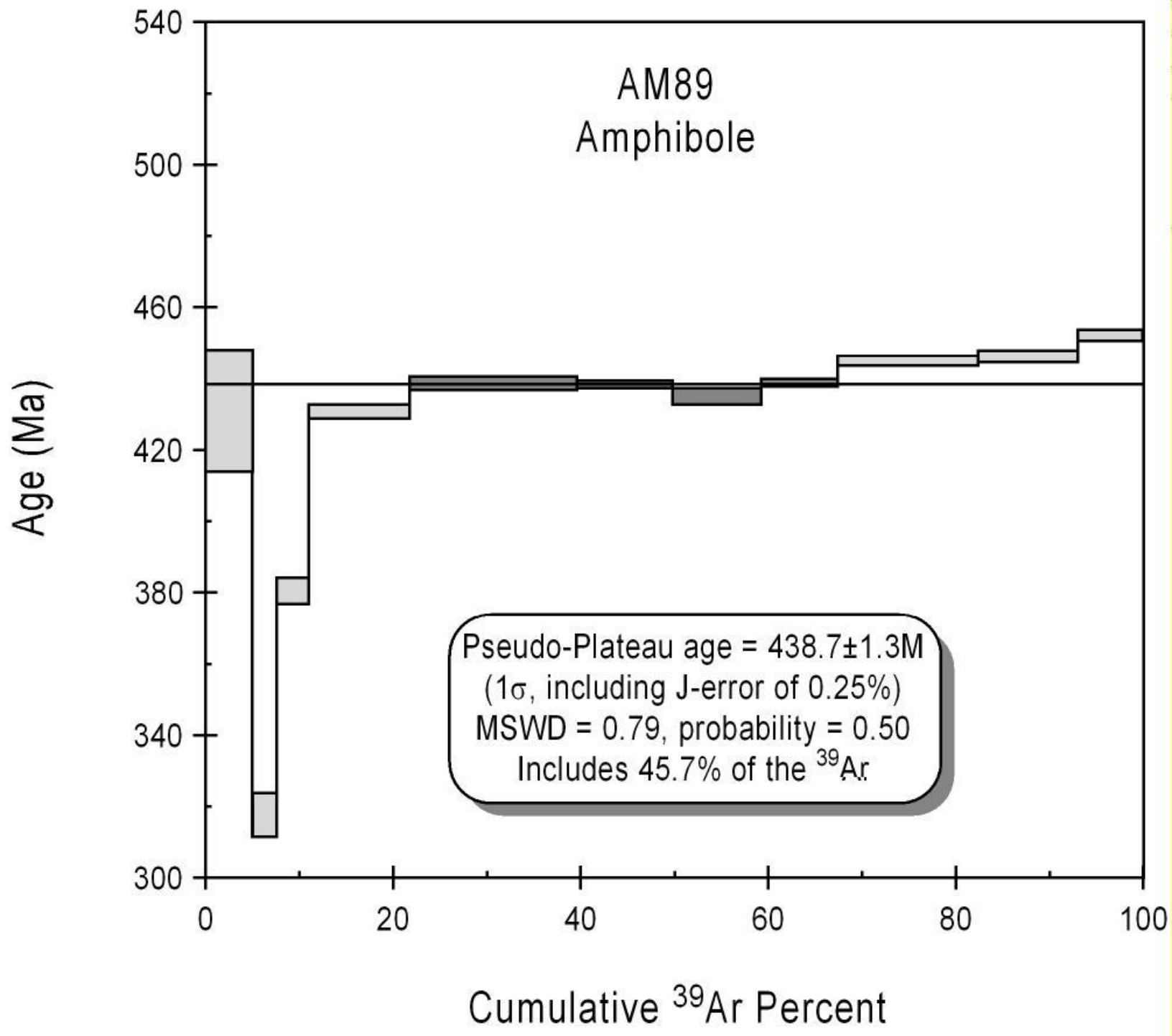


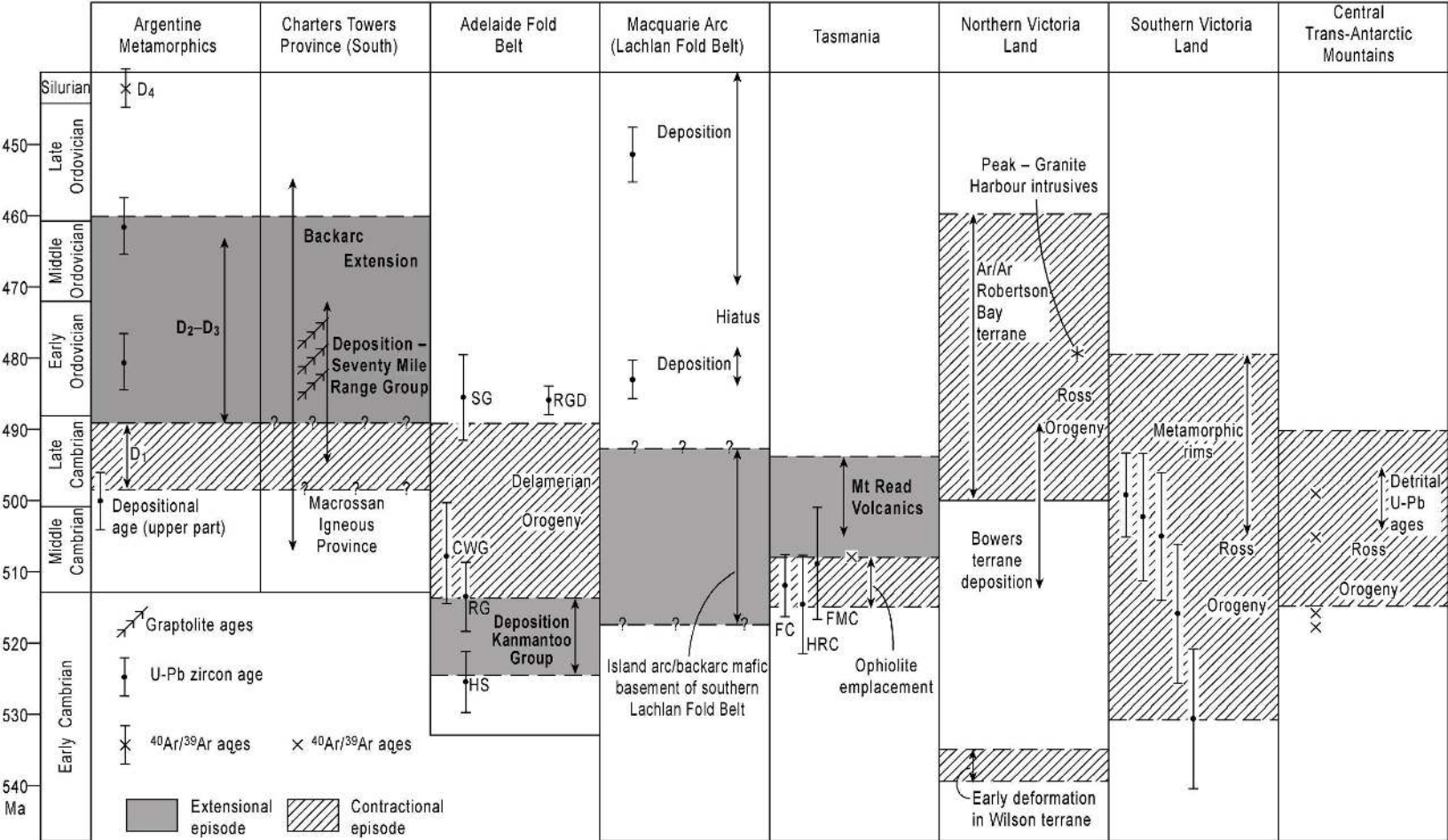
2 mm

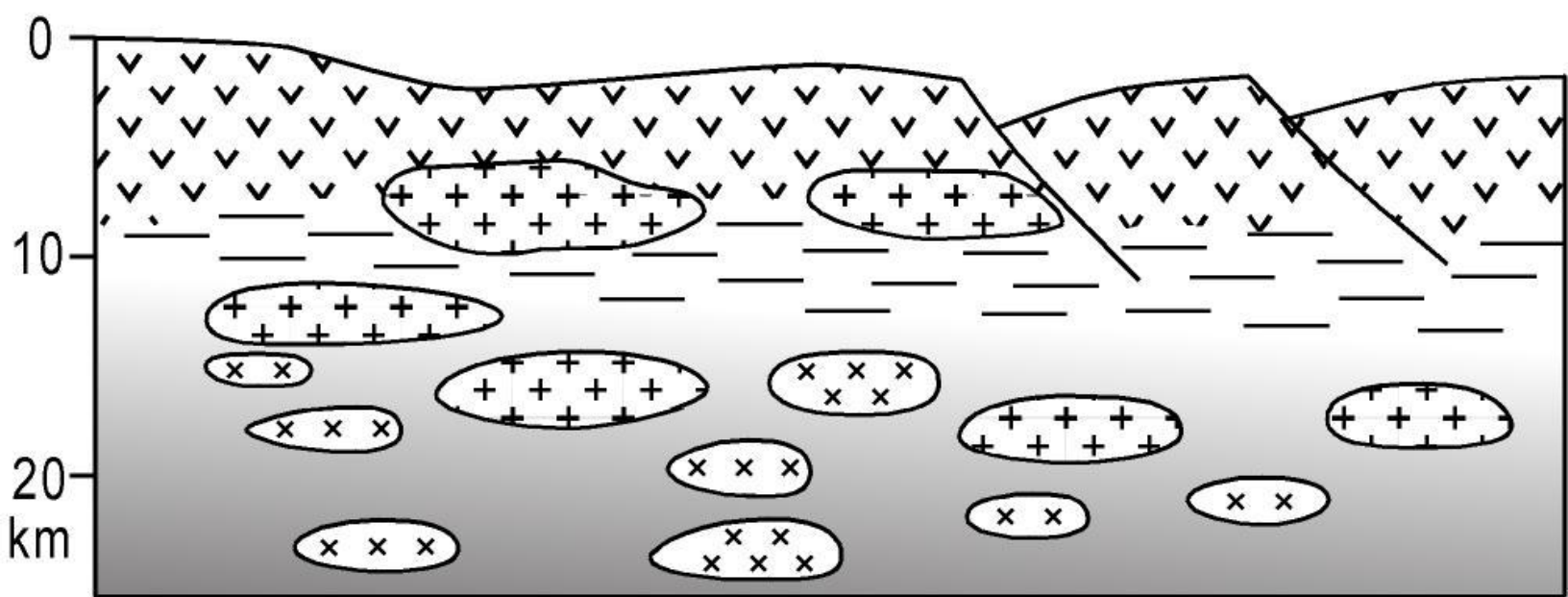


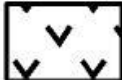
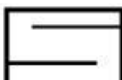
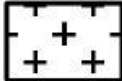
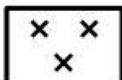





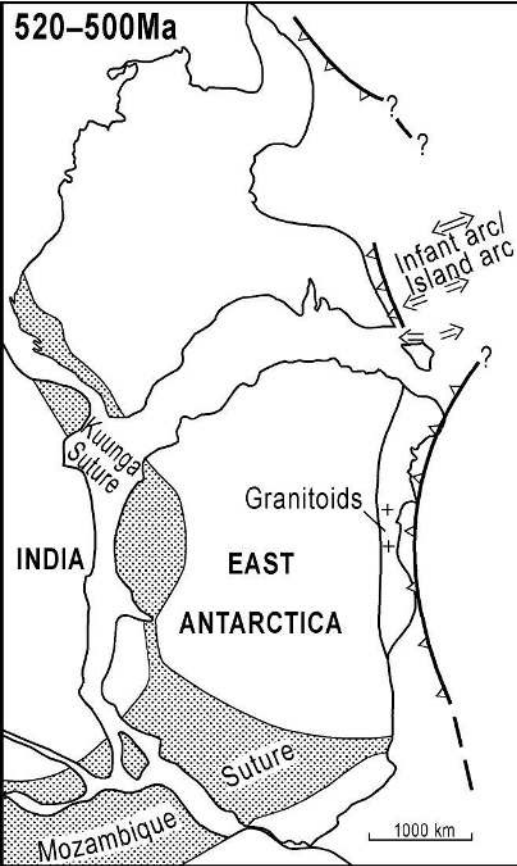




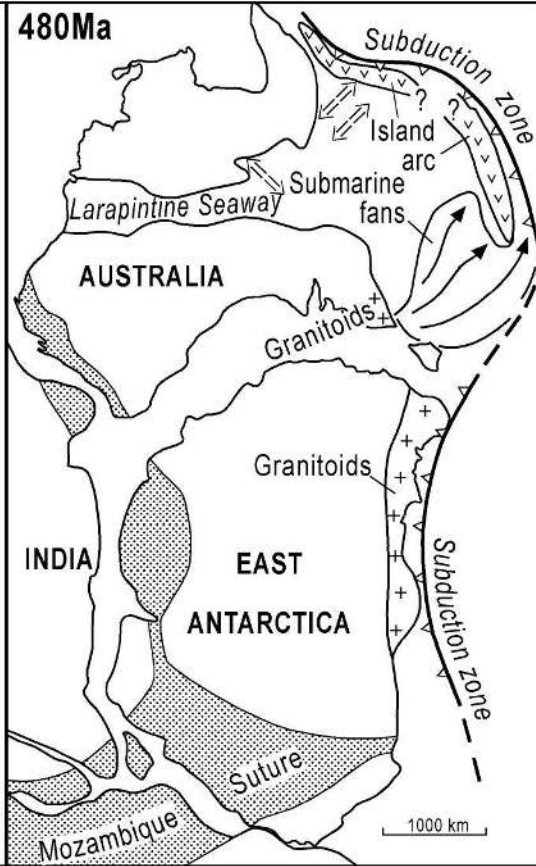


-  Silicic/mafic volcanics/volcaniclastics
 -  Fine-grained clastics
- } *Seventy Mile Range Group*
-  Granitic rocks
 -  Deformed granitic rocks
 -  Argentine/Cape River Metamorphics

520-500Ma



480Ma



460Ma

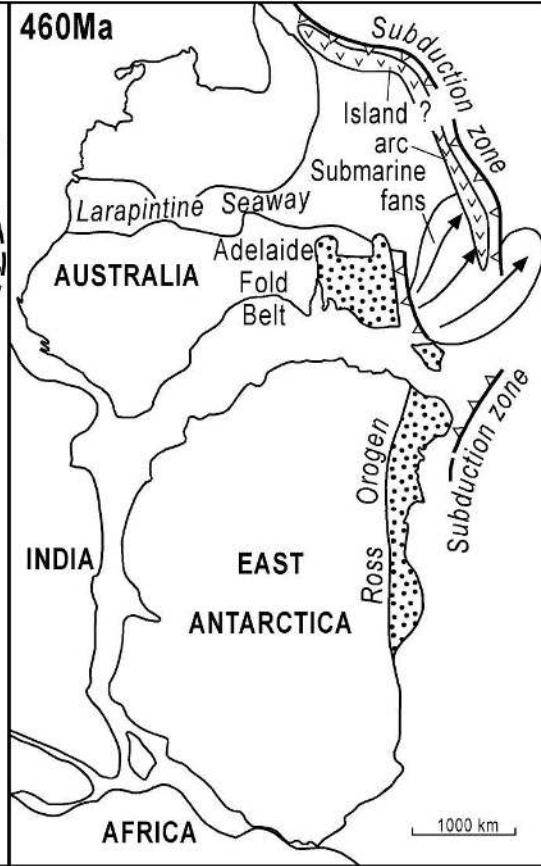


Table 1. Deformations in the Argentine Metamorphics.

Deformation	Elements	Orientation	Fold style	Foliation	Metamorphism	Distribution
D ₁	S ₁ , F ₁	S ₁ has initial northwest-southeast strike, strongly overprinted by S ₂	Rare intrafolial isoclinal folds	Well developed foliation and/or compositional layering with aligned mica, elongate quartz, amphibole	S ₁ synchronous with metamorphism - aligned biotite, muscovite, actinolite, and hornblende indicating greenschist to amphibolite facies	Throughout, but harder to find in higher grade rocks
D ₂	S ₂ , F ₂ , L ₂ (S ₂ - S ₁ intersection lineation), L _m (mineral lineation)	S ₂ dips moderately to gently southward (average orientation of 45°/136°, Fig. 5a), F ₂ and L ₂ plunge moderately to east-southeast (Fig. 5b), L _m plunges moderately to southeast (average trend of 60°/140°, Fig. 5c), orientation of L ₂ has probably been modified by D ₂ strain with stretching towards L _m	Abundant tight folds in S ₁ and quartz veins, F ₂ are typically developed on the hand specimen scale with the largest having half-wavelengths of 0.2 m, folds are rounded to tight	Zonal crenulation cleavage especially at lower grades with microlithons up to 1-2 cm thick, lithological layering commonly transposed subparallel to S ₂ , extension within foliation plane shown by boudinaged quartz and granitic veins	S ₂ synchronous with metamorphism - aligned biotite, muscovite, actinolite, and hornblende indicating greenschist to amphibolite facies	Throughout
D ₃	AS3 (Axial Plane), F ₃	AS3 are recumbent to gently inclined (Fig. 5d), F ₃ trends are west-northwest to east-southeast (Fig. 5e)	Close to tight, recumbent, verge to south, disharmonic, developed at mesoscopic scale only, stumpy shapes (low amplitude-to-wavelength ratios)	No S ₃ axial planar foliation	Some granitic dykes affected by F ₃	Higher grade rocks only, mostly around locality of Argentine south of Cattle Creek dome
D ₄	S ₄ , F ₄	Steep north-trending S ₄ with variably plunging F ₄ (Fig. 5f, g)	Broad to tight, low amplitude-to-wavelength ratios, developed at hand specimen scale but range up to folds with wavelength of 2 m	Poorly developed axial planar foliation in F ₄ hinges, S ₂ reactivated as S ₄ on limbs of F ₄ hinges	Veins of leucogranite ascribed to anatexis are both folded by F ₄ and cut across F ₄ axial planes indicating that high-grade metamorphism progressed beyond deformation	Higher grade rocks only, particularly in the western part of the Argentine area

Table 2. Temperatures calculated using the titanium oxide thermometer of *Foster* [in press]. Values are averages and ranges given in brackets reflect variation in mineral analyses and its influence on calculated temperatures.

Sample	Location	Rock type	mineral grains analysed	°C	Significance
Metaplutonic rocks - North					
IWT454	A1	419850 7857150 Amphibolite	4	732 (722-749)	Relict igneous T
IWT630	A2	420450 7859000 Amphibolite	4	767 (746-777)	Relict igneous T
IWAM089	A11	420625 7856759 Amphibolite	3	735 (701-765)	Relict igneous T
Argentine and Dome					
AM91		420977 7853099 Amphibolite	3	573 (533-611)	Metamorphic T
AM89		420740 7856933 Amphibolite	4	739 (710-750)	Relict igneous T
AM111		424088 7850288 Amphibolite	4	550 (519-578)	Metamorphic T
IWAM111	A10	423969 7850115 Amphibolite	4	564 (528-598)	Metamorphic T
Paynes Lagoon					
AM43		410839 7848825 Amphibolite	4	645 (616-661)	Hybrid T
IWT712	A3	406950 7847650 Amphibolite	3	586 (574-592)	Metamorphic T
IWT712	A4	406950 7847650 Amphibolite	4	541 (516-562)	Metamorphic T
TMR0200	A5	408450 7848250 Calc-silicate	4	628 (621-631)	Hybrid T
TMR0217	A9	406350 7846700 Amphibolite	4	549 (529-580)	Metamorphic T
Paynes Lagoon (west)					
TMR0173	A6	395850 7848250 Calc-silicate	4	626 (608-644)	Hybrid T
Towns Creek					
TMR0139	A7	397650 7864750 Amphibolite	3	547 (543-555)	Metamorphic T
TMR0139	A8	397650 7864750 Amphibolite	4	562 (543-593)	Metamorphic T

Table 3. Summary of SHRIMP U-Pb zircon results for sample IWAM162D.

Grain. spot	U (ppm)	Th (ppm)	Th/U	²⁰⁶ Pb* (ppm)	²⁰⁴ Pb/ ²⁰⁶ Pb	f ₂₀₆ %	Total				Radiogenic		Age (Ma)	
							²³⁸ U/ ²⁰⁶ Pb	±	²⁰⁷ Pb/ ²⁰⁶ Pb	±	²⁰⁶ Pb/ ²³⁸ U	±	²⁰⁶ Pb/ ²³⁸ U	±
1.1	281	180	0.64	19.0	0.000065	<0.01	12.721	0.150	0.0567	0.0008	0.0786	0.0009	487.9	5.7
2.1	171	94	0.55	12.1	0.000040	<0.01	12.140	0.390	0.0569	0.0010	0.0824	0.0027	510.6	16.0
3.1	165	90	0.54	11.4	0.000023	0.13	12.417	0.160	0.0582	0.0010	0.0804	0.0011	498.7	6.3
4.1	269	170	0.63	18.4	0.000174	0.12	12.571	0.150	0.0580	0.0009	0.0794	0.0010	492.8	5.8
5.1	123	62	0.51	8.7	-	0.15	12.110	0.165	0.0587	0.0015	0.0825	0.0012	510.8	6.9
6.1	174	99	0.57	11.8	0.000291	<0.01	12.587	0.221	0.0562	0.0010	0.0795	0.0014	493.3	8.5
7.1	132	75	0.56	9.3	0.000364	<0.01	12.237	0.166	0.0573	0.0011	0.0817	0.0011	506.4	6.7
8.1	209	119	0.57	14.4	0.000056	0.11	12.404	0.154	0.0581	0.0009	0.0805	0.0010	499.3	6.1
9.1	273	169	0.62	18.9	-	0.08	12.393	0.147	0.0579	0.0008	0.0806	0.0010	499.8	5.8
10.1	298	206	0.69	20.2	-	0.10	12.651	0.149	0.0578	0.0008	0.0790	0.0009	489.9	5.6
11.1	282	194	0.69	19.4	0.000077	0.02	12.528	0.153	0.0572	0.0008	0.0798	0.0010	495.0	5.9
12.1	584	482	0.83	40.2	0.000077	<0.01	12.475	0.137	0.0566	0.0005	0.0802	0.0009	497.4	5.3
13.1	299	247	0.83	20.9	0.000057	<0.01	12.252	0.148	0.0573	0.0008	0.0816	0.0010	505.9	6.0
14.1	183	108	0.59	12.8	0.000127	0.05	12.287	0.156	0.0578	0.0010	0.0813	0.0011	504.1	6.3
15.1	205	125	0.61	14.2	-	0.08	12.414	0.154	0.0578	0.0009	0.0805	0.0010	499.1	6.1
16.1	291	193	0.66	20.3	0.000029	0.03	12.334	0.143	0.0575	0.0007	0.0811	0.0010	502.4	5.7
17.1	266	161	0.60	18.4	0.000069	<0.01	12.443	0.169	0.0558	0.0008	0.0805	0.0011	499.1	6.6
18.1	276	194	0.70	18.9	0.000101	0.10	12.556	0.148	0.0578	0.0008	0.0796	0.0010	493.5	5.7
19.1	207	114	0.55	14.5	0.000074	0.26	12.264	0.149	0.0594	0.0009	0.0813	0.0010	504.1	6.0
20.1	834	714	0.86	59.2	0.000022	0.07	12.091	0.128	0.0581	0.0006	0.0827	0.0009	511.9	5.3
21.1	376	241	0.64	26.1	0.000052	<0.01	12.396	0.140	0.0567	0.0006	0.0807	0.0009	500.5	5.5

Notes: 1. Uncertainties given at the one σ level.

2. Error in FC1 reference zircon calibration was 0.39% for the analytical session

(not included in above errors but required when comparing data from different mounts).

3. f₂₀₆ % denotes the percentage of ²⁰⁶Pb that is common Pb.

4. Correction for common Pb made using the measured ²³⁸U/²⁰⁶Pb and ²⁰⁷Pb/²⁰⁶Pb ratios as outlined in *Williams* [1998] and references therein.

Table 4. Summary of SHRIMP U-Pb zircon results for sample HR1.

Grain. spot	U (ppm)	Th (ppm)	Th/U	²⁰⁶ Pb* (ppm)	²⁰⁴ Pb/ ²⁰⁶ Pb	f ₂₀₆ %	Total				Radiogenic		Age (Ma)	
							²³⁸ U/ ²⁰⁶ Pb	±	²⁰⁷ Pb/ ²⁰⁶ Pb	±	²⁰⁶ Pb/ ²³⁸ U	±	²⁰⁶ Pb/ ²³⁸ U	±
1.1	244	243	0.99	16.2	0.000113	0.07	12.930	0.151	0.0573	0.0008	0.0773	0.0009	479.9	5.5
2.1	202	122	0.61	13.4	0.000125	0.06	12.911	0.155	0.0572	0.0008	0.0774	0.0009	480.7	5.7
3.1	289	189	0.65	19.3	0.000005	<0.01	12.887	0.152	0.0563	0.0008	0.0776	0.0009	482.0	5.6
4.1	264	137	0.52	17.4	0.000050	0.06	13.034	0.152	0.0571	0.0009	0.0767	0.0009	476.3	5.5
5.1	300	95	0.32	10.2	0.000342	1.00	25.393	0.303	0.0592	0.0010	0.0390	0.0005	246.5	2.9
6.1	203	120	0.59	13.6	0.000246	0.33	12.840	0.155	0.0595	0.0009	0.0776	0.0010	481.9	5.7
7.1	159	98	0.62	10.6	0.000007	0.34	12.928	0.163	0.0595	0.0010	0.0771	0.0010	478.7	5.9
8.1	413	262	0.63	27.3	0.000064	0.18	12.986	0.144	0.0581	0.0009	0.0769	0.0009	477.4	5.2
9.1	324	142	0.44	21.5	0.000058	0.02	12.926	0.147	0.0569	0.0007	0.0773	0.0009	480.3	5.4
10.1	591	359	0.61	27.9	0.001802	4.13	18.205	0.198	0.0863	0.0008	0.0527	0.0006	330.8	3.6
11.1	152	78	0.51	10.4	0.002603	4.07	12.504	0.160	0.0896	0.0013	0.0767	0.0010	476.5	6.0
12.1	190	158	0.84	12.5	-	0.04	13.073	0.161	0.0569	0.0009	0.0765	0.0010	475.0	5.7
13.1	151	81	0.54	9.9	0.000766	2.26	13.108	0.167	0.0746	0.0027	0.0746	0.0010	463.6	6.0
14.1	138	62	0.45	9.3	0.000242	0.01	12.742	0.171	0.0570	0.0011	0.0785	0.0011	487.0	6.4
15.1	353	182	0.52	23.9	0.000053	0.08	12.728	0.143	0.0575	0.0006	0.0785	0.0009	487.2	5.4
16.1	252	194	0.77	16.2	0.000171	0.03	13.371	0.158	0.0566	0.0008	0.0748	0.0009	464.8	5.4
17.1	416	170	0.41	27.3	0.000138	<0.01	13.074	0.149	0.0564	0.0006	0.0765	0.0009	475.2	5.3
18.1	109	60	0.55	6.9	0.000284	0.50	13.572	0.187	0.0602	0.0013	0.0733	0.0010	456.1	6.2
19.1	196	164	0.83	13.4	0.000102	0.01	12.607	0.153	0.0571	0.0009	0.0793	0.0010	492.0	5.9
20.1	516	470	0.91	35.5	0.000051	<0.01	12.490	0.136	0.0561	0.0005	0.0802	0.0009	497.1	5.3

- Notes: 1. Uncertainties given at the one σ level.
2. Error in AS3 reference zircon calibration was 0.55% for the analytical session.
(not included in above errors but required when comparing data from different mounts).
3. f₂₀₆ % denotes the percentage of ²⁰⁶Pb that is common Pb.
4. Correction for common Pb made using the measured ²³⁸U/²⁰⁶Pb and ²⁰⁷Pb/²⁰⁶Pb ratios as outlined in *Williams* [1998] and references therein.

Table 5. Summary of SHRIMP U-Pb zircon results for sample AM77.

Grain. spot	U (ppm)	Th (ppm)	Th/U	²⁰⁶ Pb* (ppm)	²⁰⁴ Pb/ ²⁰⁶ Pb	f ₂₀₆ %	Total				Radiogenic		Age (Ma)	
							²³⁸ U/ ²⁰⁶ Pb	±	²⁰⁷ Pb/ ²⁰⁶ Pb	±	²⁰⁶ Pb/ ²³⁸ U	±	²⁰⁶ Pb/ ²³⁸ U	±
1.1	1056	450	0.43	68.4	0.000492	0.92	13.255	0.139	0.0638	0.0004	0.0748	0.0008	464.7	4.8
2.1	921	383	0.42	62.1	0.001463	2.82	12.733	0.137	0.0794	0.0009	0.0763	0.0008	474.1	5.0
2.2	812	217	0.27	55.1	0.006598	12.72	12.653	0.134	0.1584	0.0044	0.0690	0.0009	430.0	5.3
3.1	1331	846	0.64	80.4	0.002943	5.23	14.223	0.155	0.0974	0.0009	0.0666	0.0007	415.8	4.5
4.1	1029	399	0.39	64.8	0.000241	0.48	13.648	0.144	0.0599	0.0005	0.0729	0.0008	453.7	4.7
5.1	1490	688	0.46	82.5	0.006455	11.97	15.516	0.167	0.1501	0.0008	0.0567	0.0006	355.7	3.9
6.1	728	304	0.42	46.9	0.000420	0.60	13.347	0.146	0.0611	0.0005	0.0745	0.0008	463.1	5.0
6.2	840	304	0.36	52.7	0.000034	0.17	13.698	0.146	0.0574	0.0005	0.0729	0.0008	453.5	4.7
7.1	1053	420	0.40	67.8	0.002258	4.00	13.343	0.140	0.0883	0.0005	0.0719	0.0008	447.9	4.6
8.1	948	391	0.41	61.1	0.002723	4.86	13.315	0.141	0.0952	0.0009	0.0715	0.0008	444.9	4.7
9.1	1338	645	0.48	93.2	0.003400	5.90	12.332	0.130	0.1044	0.0007	0.0763	0.0008	474.0	4.9
10.1	940	449	0.48	62.8	0.000975	1.93	12.864	0.137	0.0722	0.0005	0.0762	0.0008	473.7	4.9
11.1	845	356	0.42	54.3	0.001365	2.50	13.362	0.142	0.0763	0.0005	0.0730	0.0008	454.0	4.7
12.1	850	285	0.34	54.5	0.000693	1.19	13.402	0.142	0.0658	0.0005	0.0737	0.0008	458.6	4.8
13.1	1286	551	0.43	82.9	0.000905	1.82	13.324	0.140	0.0709	0.0004	0.0737	0.0008	458.3	4.7
14.1	985	538	0.55	63.2	0.000147	0.25	13.389	0.141	0.0583	0.0004	0.0745	0.0008	463.2	4.8
15.1	1112	392	0.35	70.5	0.001754	3.14	13.550	0.142	0.0813	0.0016	0.0715	0.0008	445.1	4.7
16.1	1346	376	0.28	132.2	0.027821	50.29	8.747	0.092	0.4597	0.0058	0.0568	0.0015	356.3	9.1
17.1	1053	547	0.52	68.0	0.000016	0.04	13.301	0.149	0.0567	0.0004	0.0752	0.0009	467.1	5.1
18.1	1020	458	0.45	66.3	0.000124	0.22	13.216	0.139	0.0582	0.0004	0.0755	0.0008	469.2	4.8
19.1	927	426	0.46	59.9	0.000634	1.28	13.295	0.141	0.0666	0.0005	0.0743	0.0008	461.7	4.8
20.1	826	365	0.44	52.9	0.000022	-0.09	13.418	0.155	0.0556	0.0004	0.0746	0.0009	463.8	5.3
21.1	1191	640	0.54	74.7	0.003217	5.69	13.696	0.143	0.1014	0.0005	0.0689	0.0007	429.3	4.4
22.1	868	477	0.55	56.0	0.000231	0.59	13.314	0.157	0.0611	0.0005	0.0747	0.0009	464.2	5.4
23.1	1216	330	0.27	68.5	0.001789	3.04	15.238	0.160	0.0792	0.0005	0.0636	0.0007	397.7	4.1

Notes: 1. Uncertainties given at the one σ level.

2. Error in FC1 Reference zircon calibration was 0.57% for the analytical session
(not included in above errors but required when comparing data from different mounts).
3. f₂₀₆ % denotes the percentage of ²⁰⁶Pb that is common Pb.
4. Correction for common Pb made using the measured ²³⁸U/²⁰⁶Pb and ²⁰⁷Pb/²⁰⁶Pb ratios
as outlined in *Williams* [1998] and references therein.

Table 6. $^{40}\text{Ar}/^{39}\text{Ar}$ step-heating analytical results for sample AM89 (amphibolite).

Temp (C)	Cum % ^{39}Ar	$^{40}\text{Ar}/^{39}\text{Ar}$	$^{37}\text{Ar}/^{39}\text{Ar}$	$^{36}\text{Ar}/^{39}\text{Ar}$	Vol. ^{39}Ar $\times 10^{-14}$ mol	%Rad. ^{40}Ar	Ca/K	$^{40}\text{Ar}^*/^{39}\text{Ar}$	Age (Ma)	\pm 1s.d. (Ma)
AM89 Hornblende										
J-value = 0.018839 ± 0.000047										
800	4.91	80.10	1.4511	0.2229	1.022	17.9	2.76	14.32	431.0	16.8
900	7.53	25.06	3.1637	0.0510	0.544	40.8	6.02	10.24	318.2	6.0
980	11.16	18.62	5.1496	0.0223	0.759	66.8	9.82	12.48	380.9	3.6
1010	21.97	15.64	5.7251	0.0061	2.255	91.3	10.90	14.33	431.2	1.8
1040	39.77	15.10	5.8923	0.0034	3.715	96.5	11.20	14.63	439.2	1.7
1070	49.86	15.04	5.8927	0.0032	2.106	96.8	11.20	14.62	438.8	1.2
1100	59.41	14.95	5.9910	0.0034	1.993	96.5	11.40	14.48	435.3	2.4
1130	67.63	15.13	6.0629	0.0035	1.717	96.3	11.60	14.63	439.1	1.1
1170	82.60	15.32	6.0467	0.0033	3.124	96.7	11.50	14.86	445.4	1.4
1200	93.24	15.38	6.0558	0.0034	2.221	96.5	11.60	14.91	446.7	1.5
1450	100.00	17.72	6.2240	0.0106	1.411	85.0	11.90	15.13	452.4	1.6
Total		18.95	5.6445	0.0168	20.87			14.47	435.0	2.5

i) Errors are one sigma uncertainties and exclude uncertainties in the J-value.

ii) Data are corrected for mass spectrometer backgrounds, discrimination and radioactive decay, but not isotopic interferences.

iii) Interference corrections: $(^{30}\text{Ar}/^{39}\text{Ar})_{\text{Ca}} = 2.79(\pm 0.05) \times 10^{-4}$; $(^{33}\text{Ar}/^{39}\text{Ar})_{\text{Ca}} = 6.82(\pm 0.05) \times 10^{-4}$; $(^{40}\text{Ar}/^{39}\text{Ar})_{\text{K}} = 2.86(\pm 0.06) \times 10^{-4}$

iv) J-value is based on an age of 1072 Ma for Hb3gr hornblende [Turner *et al.*, 1971].